

Electroweak high-energy scattering and the chiral anomaly

Alan R. White*

Argonne National Laboratory, 9700 South Cass, Illinois 60439, USA

(Received 17 October 2003; published 19 May 2004)

The effect of perturbative QCD interactions on the high-energy scattering of electroweak vector bosons, when the exchanged channel has pion quantum numbers, is considered. The chiral anomaly is shown to appear in the couplings of particular transverse momentum diagrams, producing an enhancement of the scattering amplitude by a power of the energy. At $O(\alpha_s)$ a single large transverse momentum gluon is involved and, within the transverse momentum diagram framework, there is no cancellation. In higher orders, soft gluons, carrying both normal and anomalous color parity, are also present. The manipulation of a transverse momentum cutoff to replace the ultraviolet anomaly divergence by infrared divergences that can lead to confinement and chiral symmetry breaking is briefly discussed. The possible implications for electroweak symmetry breaking are noted.

DOI: 10.1103/PhysRevD.69.096002

PACS number(s): 11.15.Bt, 11.55.Jy

I. INTRODUCTION

The cancellation of the chiral anomaly in the electroweak sector of the standard model is crucial for the existence of the model as a well-defined short-distance field theory. In perturbation theory, the anomaly is a large momentum contribution in axial vector triangle diagrams that, if uncancelled, destroys the renormalizability of a left-handed gauge theory such as the electroweak sector of the standard model. In the Regge limit the Feynman diagrams of standard perturbation theory contract to form transverse momentum diagrams and produce a new perturbation expansion that can be organized into Reggeon diagrams [1–7]. Beyond leading-log order, the external couplings of the transverse momentum diagrams (which are also the couplings of the Reggeon diagrams) contain contracted loop diagrams involving “effective vertices” that result from the contraction. The effective vertices can then produce new “anomalies,” not present in the normal perturbation expansion. For QCD, this is demonstrated in the next-to-leading log calculation [4] of gluon scattering, in which an infrared (gluon) triangle anomaly is responsible for the helicity nonconservation that occurs, and in our work on the contribution of infrared quark loop anomalies to pion or Pomeron [8] and triple Pomeron [9] vertices.

In the electroweak scattering problem considered in this paper, the underlying left-handed theory contains elementary axial vector vertices. It is natural, therefore, that (components of) these elementary vertices will appear also in the Regge limit effective vertices. *A priori*, therefore, large momentum contributions, directly analogous to the familiar triangle anomaly, can be expected within the loop diagrams that contribute to (beyond-leading-order) transverse momentum diagram couplings. Indeed, as we shall see, internal effective vertices, resulting from longitudinal vector meson exchange, also appear which are quark current components that have point interactions only at infinite momentum. Such current components do not appear in the original Lagrangian

and do not couple to leptons. Consequently, in the electroweak Regge limit, we can anticipate a significantly expanded “anomaly problem” which the well-known short distance cancellations, between quarks and leptons, will not be sufficient to remove.

In this paper we will show that the triangle anomaly does indeed appear in the couplings of transverse momentum diagrams that describe the high-energy scattering of $W^{\pm,0}$ vector mesons. All the diagrams we consider describe the exchange of a quark-antiquark pair, with the flavor quantum numbers of the pion, together with some number of gluons. We choose pion quantum numbers because our ultimate goal is to understand the relationship between the anomaly and chiral symmetry breaking in the context of high-energy scattering. Since two fermion exchange is involved, we would expect the energy dependence to be, at most, logarithmic. (Pion exchange would have no energy dependence.) The signal of the anomaly will be a power divergence of transverse momentum integrals that produces an additional power of the energy in the full amplitude.

Since the anomaly phenomenon we discuss involves longitudinal vector meson states it is natural to expect that the underlying gauge invariance of the electroweak theory will be responsible for some form of cancellation. We discuss this possibility at some length in an appendix at the end of the paper. While it appears that the anomaly is not completely eliminated, these identities do produce cancellations that can not be straightforwardly expressed in terms of transverse momentum diagram divergences. Moreover, it is clear that the large transverse momentum region producing the anomaly could also contribute in an important way within superficially nonleading Feynman diagrams. If there is finally a cancellation, then it most likely means the failure of the transverse momentum diagram formalism for the electroweak theory unless (as, in any case, we strongly advocate) a transverse momentum cutoff is imposed from the outset. In the main body of the paper our purpose will be to study contributions to transverse momentum diagrams and, apart from the discussion in Appendix D, and the related discussion in Sec. V C, we will make only brief references to the possibility that there could be important contributions out-

*Email address: arw@hep.anl.gov

side of the transverse momentum diagram formalism.

The anomaly occurs only in the even signature amplitude, which is a sum of scattering amplitudes for vector mesons with opposite and same sign helicities, i.e.,

$$\begin{aligned} A^+(S) &= A^+(P_+P_-) = A_{-+}(P_+,P_-) + A_{++}(-P_+,P_-) \\ &= A_{-+}(S) + A_{++}(-S). \end{aligned} \quad (1.1)$$

with

$$A_{-+}(S) \xrightarrow[S \rightarrow \infty]{} cS, \quad A_{++}(S) \xrightarrow[S \rightarrow \infty]{} -cS. \quad (1.2)$$

In a vector theory the amplitudes $A_{-+}(S)$ and $A_{++}(S)$ would simply add in a single helicity amplitude and the anomaly would cancel.

Our calculations are carried out in a theory that is very close to, but is not quite, the standard model. For simplicity, as we discuss further in Sec. II, we ignore both leptons and the photon and consider only one doublet of quarks. We discuss the general framework for our analysis in Sec. III and isolate the simplest diagram, which is $O(\alpha_s)$, that potentially gives an enhancement. Section IV is devoted to a detailed demonstration that the enhancement does indeed occur in this diagram. It is generated by the combination of an effective vertex due to the left-handed coupling of a scattering vector meson, a quark-antiquark effective vertex due to a longitudinal massive vector intermediate state, and a single (large transverse momentum) gluon vertex. At $O(\alpha_s)$, there is only a small number of possibilities for the anomaly to occur within the transverse momentum diagram formalism and, as we discuss in Sec. V, it is clear that it does not cancel.

As we show in Sec. VI, at $O(\alpha_s^2)$ there are contributions in which an additional soft gluon plays no kinematical role in the occurrence of the anomaly and simply accompanies the $O(\alpha_s)$ process. Not surprisingly, the soft gluon produces a transverse momentum infrared divergence in individual diagram contributions. In tracing the corresponding cancellation, we find new (but closely related) processes which occur first only at $O(\alpha_s)^2$ and for which infrared properties of the anomaly are needed to fully determine their contribution. Also at $O(\alpha_s^2)$, ‘‘anomalous’’ (odd) color charge parity two gluon exchange appears, involving one finite and one large transverse momentum gluon.

In this paper we will frequently refer to a multigluon transverse momentum state which carries color zero and anomalous color charge parity (not equal to the gluon number) as ‘‘anomalous gluons.’’ In the present context, such a state first appears at $O(\alpha_s^3)$. Three gluons with even color parity and (separately) large, finite, and soft transverse momentum are involved. In higher orders various combinations of soft and finite transverse momentum gluons can accompany the large transverse momentum gluon. Additional gluons could also share the large transverse momentum, but we do not discuss this possibility.

Reggeized gluon exchanges that are the outcome of perturbative calculations [1–7] in a vector theory carry normal color parity (even/odd for an even/odd number of gluons). However, we have argued (for a very long time [10]) that

anomalous gluons play a crucial role [8] in the emergence of QCD confinement and chiral symmetry breaking, in the context of high-energy scattering and Reggeon diagrams. In particular, we have argued that the Pomeron is formed from anomalous gluons and that configurations of this kind are an essential component of Regge limit pions and nucleons. However, while we have been able to show how [9] anomalies provide triple Pomeron and pion-Pomeron interactions involving the anomalous gluons, it has proven very difficult to find a simple starting point in which the anomalous gluons couple directly and from which a detailed description of hadron amplitudes can be developed. It is very encouraging, therefore, to see that anomalous gluons appear straightforwardly in the anomaly contributions that dominate the electroweak scattering amplitudes we consider.

We have not explored the full consequences of the power enhancement (1.2) nor, as we discussed above, is it clear that the possibilities for cancellation have been exhausted. While no unitarity bound is violated, we, nevertheless, believe that the enhancement severely threatens the unitarity of the theory (at least in the t channel) and should not be present in physical amplitudes. Rather than looking for further cancellations, we will argue (only very briefly in this paper) that although the enhancement is actually unphysical, it selects the physically relevant diagrams and, in doing so, anticipates chiral symmetry breaking and confinement. In fact there is no sign, in the anomaly amplitudes that give Eq. (1.2), of either the s -channel or the t -channel intermediate states that are present in the diagrams from which they are calculated. In Sec. VII, we suggest that the enhancement is obtained by using a ‘‘wrong procedure’’ to evaluate the Regge limit contribution of diagrams. If a transverse momentum cutoff is initially imposed, the energy enhancement will be eliminated. Instead, because the cutoff produces a Ward identity violation, the anomaly diagrams dominate because of infrared transverse momentum divergences that appear and infrared properties of the anomaly come into play. We will argue that these divergences should be analyzed, and ‘‘physical amplitudes’’ extracted, before the cutoff is removed. This is emphasized as a major conclusion of the paper in Sec. VIII, which also contains other conclusions.

Initially, a study of the infrared anomaly contributions of diagrams, that matches the present study of ultraviolet contributions, will be required. After this, we anticipate, the analysis of infrared divergences will parallel our discussion [8] of hadron scattering. All-orders properties of the divergences have to be combined with Reggeon field theory, to obtain the ‘‘physical amplitudes’’ in which the cutoff can be removed. In this paper we will describe only the general arguments that we believe should be employed. We expect that the resulting amplitudes will have both confinement and chiral symmetry breaking, in the sense that the scattering will be describable as the exchange of a color zero, Goldstone boson, pion. Although our hadron work provides the framework for our general understanding, a major part of the logic and justification for the procedure we outline can be appreciated directly within the present context, without reference to the Pomeron problem. That the starting point is

much more straightforward than in the hadron case holds out the promise that it will be correspondingly easier to carry the procedure through in detail.

II. THE ALMOST STANDARD MODEL

For simplicity, we will consider a theory which, for our purposes, is sufficiently close to the standard model, but which is actually less complex. We will consider a “flavor SU(2)” triplet of vector mesons $\{W^+, W^-, W^0\}$ with mass M and left-handed couplings to a flavor doublet of quarks $\{u, d\}$ with the usual QCD interaction. We will effectively assume that the vector mesons originate from a spontaneously broken gauge theory, as in the standard model, but apart from the discussion of Reggeization in this section, their self-interaction will play almost no role in our analysis. (There will be no gauge dependence in our discussion because the vector mesons will always be on shell and gluons will only contribute in gauge-independent transverse momentum diagrams—although, in effect, we evaluate gluon contributions in the Feynman gauge.)

We ignore the extra complications of the photon and all mixing angles, which could only lessen the possibilities for cancellation of the anomaly phenomenon that we find. Since there is no photon, the usual electroweak ultraviolet anomaly is absent and so we do not need to include leptons. In fact, as we noted in the Introduction, the anomaly we discuss involves (components of) QCD currents to which leptons do not couple and, therefore, could not provide any possibility for cancellation. If we give the quarks a small mass m ($\ll M$) any potentially singular infrared contributions will be eliminated. However, for much of our discussion we will be interested only in large internal (transverse) momenta, where “large” is defined relative to M , and so m will be omitted. The absence of a quark mass has the technical advantage that we will be able to exploit the considerable, Regge limit, simplifications of the Feynman diagrams that describe a massless chiral theory.

We will study the high-energy scattering of the massive vector mesons via a quark-antiquark exchange channel in which, potentially, a “pion” could appear as a bound state. Perturbatively, the leading behavior of the amplitudes we study would be given (if there were no anomaly enhancement) by the exchange of vector mesons. However, since the flavor symmetry is non-Abelian, the vector mesons will be Reggeized by self-interactions. Since CP is conserved, signature is well-defined and Reggeized vector meson exchange will give high-energy behavior in the odd-signature channel of the form

$$A(S,0) \underset{S \rightarrow \infty}{\sim} S^{\alpha(0)}, \tag{2.1}$$

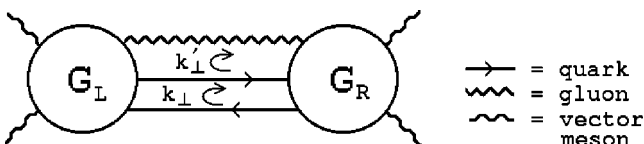


FIG. 1. A transverse momentum diagram.

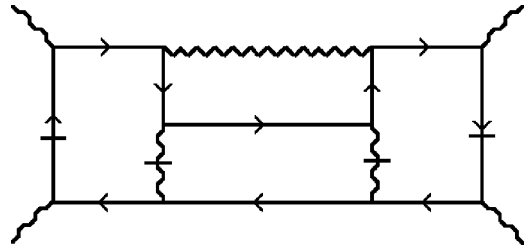


FIG. 2. A Feynman diagram—the hatched lines are on shell.

where

$$\alpha(0) = 1 - \frac{g^2}{16\pi^2} + O(g^4) < 1. \tag{2.2}$$

The even signature channel will be dominated by the exchange of two Reggeized vector mesons for which (apart from a logarithmic factor)

$$A(S,0) \underset{S \rightarrow \infty}{\sim} S^{2\alpha(0)-1} < S^{\alpha(0)}. \tag{2.3}$$

Therefore, if we sum (in principle at least) all diagrams producing all self-interaction Reggeization effects then the contribution of (any number of) exchanged vector mesons to flavor exchange amplitudes will be smaller than the anomaly enhanced quark-antiquark exchange amplitudes we discuss which give

$$A(S,0) \underset{S \rightarrow \infty}{\sim} \frac{S}{M^2}. \tag{2.4}$$

Since the running of α_s does not enter our calculations, the relative value of M , compared to the QCD scale, does not appear in our discussion. Therefore, the instability of the vector mesons is not an issue. More generally it also should not be a very significant issue. We can, of course, define vector meson scattering amplitudes by going to complex poles and any undesirable features of these amplitudes will feed back into the scattering amplitudes of physical particles. Alternatively, we could exploit the Reggeization property of vector mesons and, although it would be very obscure for most readers, we could carry out our discussion in terms of Reggeon amplitudes. In this case, it would be rather straightforward to argue that the non-Regge nature of the anomaly enhancement energy behavior that we find will violate t -channel unitarity. However, since the simplest diagrams we consider are already very high-order in the electroweak coupling [$O(\alpha_w^4)$] their contribution is very small at current energies and so any unitarity problems could only be of physical relevance at extremely high energies.

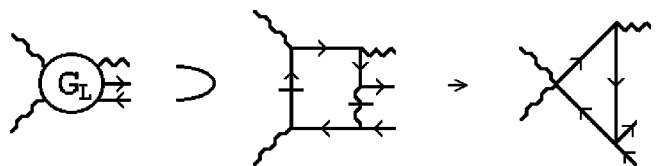
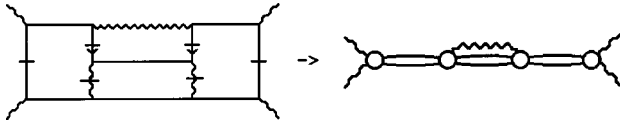


FIG. 3. A triangle diagram coupling with “effective vertices.”



$\times [\ln s]^4$

FIG. 4. The leading-log amplitude.

We could also regard our calculations as academic and say that we are simply using left-handed vector mesons to uncover properties of QCD. From this point of view we could make the mass M as small as we like. Also, throughout the main body of the paper the origin of M will be irrelevant and we will implicitly assume that it originates from some mechanism which is unrelated to the quarks we consider. It is important that the high-energy behavior (2.4) is obtained with internal vector mesons on mass shell. Because longitudinal states are involved this behavior is scaled by M^2 and so can not be cancelled by a physical Higgs contribution of any kind.

If we ignore Reggeization, or if the vector mesons are massless, then the anomaly enhanced amplitudes will give high-energy behavior comparable with that of (multiple) vector meson exchange. This could be an additional reason, to be added to those briefly mentioned in Sec. V why bound states of (higher-colored) quarks and antiquarks should actually be responsible for the vector meson mass generation. If the electroweak scale M is actually a second QCD scale, as would then be the case, we would surely expect unitarity to be just as important for the higher scale as for the lower scale.

III. $O(\alpha_s)$ —ONE GLUON DIAGRAMS

In this section we describe the general framework within which we discuss $O(\alpha_s)$ diagrams and focus on the simplest Feynman diagram that, potentially, produces an anomaly enhancement.

A. Transverse momentum diagrams

As is very well known, the leading (Regge limit) high-energy behavior of a Feynman diagram is typically obtained by routing the large light-cone momenta through the diagram in such a way that the number of particles that are close to mass shell and have large relative longitudinal momentum separations (i.e., large rapidity differences) is maximal. After longitudinal integrations are carried out, close to the on-shell configuration, the result is a transverse momentum integral multiplied by logarithms of the energy. The transverse momentum integral corresponds to a “transverse momentum diagram” obtained by contracting all of the (close to) on-shell lines. In general, there is one logarithm and one transverse momentum loop for each large rapidity difference. Consequently, the leading-log amplitude contains a transverse momentum diagram with the maximal number of loops. In Appendix B we provide a brief, nontechnical, review [11] of known results that apply to the fermion exchange scattering amplitudes we will discuss.

The relationship between transverse momentum diagrams and the process of putting lines on shell in full Feynman diagrams will dominate our discussion. When two, or more,

particles have finite relative rapidity, fewer lines are placed on shell in the reduction to a transverse momentum diagram, and a nonleading log amplitude, with a smaller number of transverse momentum loops, is obtained. In this case, the couplings and interactions in the transverse momentum diagrams have more structure. It is in (superficially) nonleading amplitudes of this kind that the high-energy behavior can be enhanced by the occurrence of the triangle anomaly within the couplings of the transverse momentum diagram.

B. Double logs

A well-known extra complication, in the application of the transverse momentum diagram formalism to fermion exchange amplitudes, is that transverse loops involving only fermion propagators are generally logarithmically divergent [11] at large transverse momentum. These divergences, effectively, produce additional logarithms of the energy and give rise to “double logs” that are associated with single rapidity differences. In the diagrams we discuss there is, potentially, a logarithmic divergence of this kind but it is overwhelmed by the anomaly power divergence that we find. Therefore, we will not be directly interested in logarithmic transverse momentum divergences and, in the main body of the paper, will refer to them only for reasons of completeness. In Appendix B we briefly discuss the possible physical relevance of the anomaly with respect to the double logs.

From the general viewpoint of this paper, however, it is important that, because we can regard the double logs as described by transverse momentum diagrams, they do not represent high-energy behavior that is not anticipated by this formalism. (Even though it might not be the most efficient method for studying properties of the double logs.) It is, perhaps, worth noting that, since the divergences do not occur in Reggeization diagrams, they do not affect the reorganization of transverse momentum diagrams into Reggeon diagrams. In fact, this reorganization reduces the degree of divergence. The divergences occur only in Reggeon diagram loops containing just Reggeized quarks and antiquarks and, if the leading log form of the trajectory function is used, the

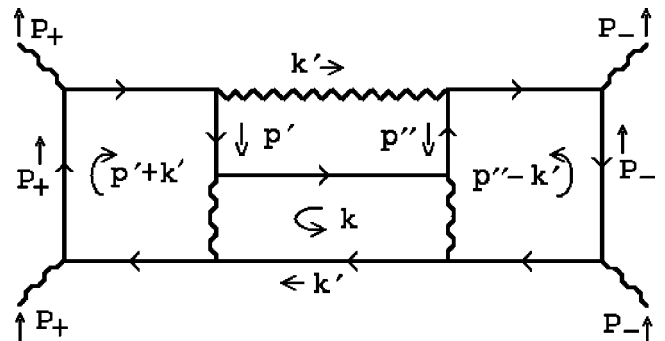


FIG. 5. Momentum notation for the diagram of Fig. 2.

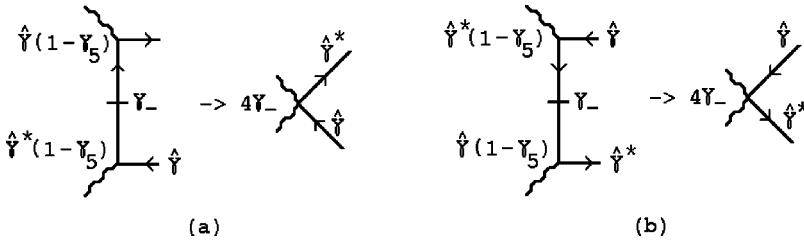


FIG. 6. Effective vertices (a) for helicity $\Lambda = -1$ (b) for helicity $\Lambda = +1$.

presence of the Reggeon propagator reduces the divergence from \log to $\log[\log]$ form.

C. The enhanced transverse momentum diagram

As we will elaborate below, the lowest-order appearance of the anomaly enhancement is associated with the transverse momentum diagram shown in Fig. 1. The remainder of this section and the following two sections will be devoted to the study of $O(\alpha_s)$ Feynman diagrams which give a contribution to the high-energy scattering of vector mesons that contains this transverse momentum integral.

We will use the diagrammatic notation of Fig. 1—for quarks, gluons, and vector mesons—throughout the paper, in both Feynman diagrams and transverse momentum diagrams. (Almost all of our discussion will be concerned with Feynman diagrams and so there should be no confusion as to which kind of diagram is under consideration.) For simplicity, in this and the following two sections, we will omit flavor and color quantum numbers and consider just the momentum and spin structure of diagrams. In this case, a “gluon” is effectively a “photon,” i.e., a massless vector particle with a vector coupling to a massless (for most of the discussion) “quark-antiquark” pair. A “vector meson” is a massive vector particle with a left-handed (right-handed) coupling to the quark (antiquark). Because of the left-handed coupling, the high-energy scattering of vector bosons with definite helicity has a particularly simple diagrammatic structure.

To avoid the introduction of an extra momentum scale, we will consider forward scattering, i.e., zero momentum transfer. We should emphasize, however, that this does not imply that our calculations are invalidated for the simple reason that we consider an infrared region in which perturbation theory does not apply. It should become clear that, since the phenomenon we discuss involves large internal transverse momenta, a momentum transfer t with $M^2 \ll t \ll S$ would not significantly affect our analysis. In the forward direction, the integrand of Fig. 1 is a product of the couplings $G_L(k_\perp, k'_\perp)$ and $G_R(k_\perp, k'_\perp)$ and transverse momentum propagators for the gluon, quark, and antiquark and the integral has the simple form

$$\int d^2k'_\perp \int d^2k_\perp \frac{\text{Tr}\{k_\perp G_L(k_\perp, k'_\perp) k_\perp G_R(k_\perp, k'_\perp)\}}{k'^2_\perp (k^2_\perp)^2}. \quad (3.1)$$

G_L and G_R should satisfy (Reggeon) Ward identities so that, as discussed further in Sec. V, there is no infrared divergence at $k'^2_\perp = 0$ and a divergence at $k^2_\perp = 0$ would be eliminated by adding either a momentum transfer or a quark mass, as discussed in the previous section. Conventionally, since two fermion exchange is involved, we would expect the accompanying energy dependence to be only logarithmic. We would also expect the large momentum behavior of G_L and G_R to be such that the full integral is, at worst, logarithmically divergent (producing an additional energy logarithm, as discussed above). The signal of the anomaly will be that G_L and G_R actually grow at large transverse momentum, in a manner that produces an additional power of the energy.

D. A Feynman graph producing the anomaly enhancement

In the next section we will see that the Feynman diagram shown in Fig. 2 has a Regge limit contribution, involving the transverse momentum diagram of Fig. 1, in which each of the hatched lines is placed on shell.

In effect, the box graphs at either end of the full graph contract to give triangle diagram contributions to the couplings G_L and G_R as shown in Fig. 3. If the left-handed nature of the interactions of the scattering vector particles leads to a left-handed (vector) “effective vertex” for the triangle diagram then, naively, it would appear that the triangle anomaly is obviously present. If this has the standard form of the ultraviolet triangle anomaly, we would expect a linear growth with k'_\perp that would then produce a divergence of the k'_\perp integration. In fact, since effective vertices are not necessarily simple local vertices or, if they are, the propagators may no longer be elementary, much more discussion is required to show that there is a contribution that is closely related to the triangle anomaly.

The diagram of Fig. 2 has the minimal complexity needed to generate triangle couplings, as in Fig. 3, for both G_L and G_R . We will find that this is necessary to obtain a nonzero contribution in the full amplitude.

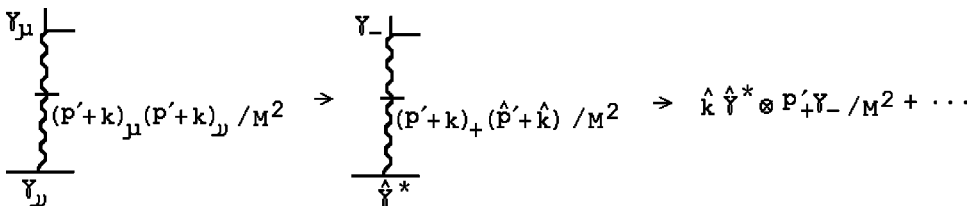


FIG. 7. The internal vector meson numerator.

E. Leading logs, nonleading logs, and the anomaly

A priori, as described in Appendix B, we expect the leading high-energy behavior of Fig. 2 to be $[\ln s]^4$, multiplied by the transverse momentum diagram obtained, as illustrated in Fig. 4, by placing all vertical lines on shell. (A hatch on a line will always imply that it is on-shell.) In fact, this transverse momentum diagram contains quark loops that are logarithmically divergent and generate additional powers of $\ln s$, as discussed above.

The transverse momentum diagram of Fig. 1 should appear at the next-to-next-to-leading log level (formally with a factor of $[\ln S]^2$). In this contribution, it would be anticipated that the dominant internal momenta, within the G_L and G_R couplings, will be “close to” that of the corresponding fast external particle (in particular, there should be no large internal rapidity difference).

The expectation would be that large (relative) internal momenta within the G_L and G_R couplings are suppressed because of Ward identity cancellations that are a consequence of gauge invariance for the gluon (giving either a finite or, at worst, logarithmically divergent integral). As we will see, the anomaly contradicts this expectation in that it is a contribution to the G_L and G_R couplings from, relatively, large internal momentum in which the unhatched vertical quark lines of Fig. 2 (and, correspondingly, the unhatched vertical line of Fig. 3) are far off shell. This does not, however, imply the failure of a Ward identity. Rather, as we enlarge on further in Sec. V, the presence of the anomaly means that large internal momenta play an important role in the Ward identity. (In Appendix C we review the corresponding situation for the vector Ward identities in the familiar axial-vector–vector–vector triangle diagram in which the anomaly occurs.)

In the course of our analysis we will find that, in the low-order diagrams where the anomaly first occurs, there are no additional logarithms (multiplying the power enhancement) associated with lines that are only close to on shell, rather than actually on shell, in the large transverse momentum divergence.

IV. THE ANOMALY ENHANCEMENT

In this section we study, in detail, the occurrence of the anomaly enhancement in the high-energy behavior of the Feynman diagram of Fig. 2. This diagram is shown again in Fig. 5, together with the momentum notation that we will use.

We will consider the limit

$$P_+ \rightarrow \left(\frac{\sqrt{S}}{2}, \frac{\sqrt{S}}{2}, 0, 0 \right), \quad P_- \rightarrow \left(\frac{\sqrt{S}}{2}, -\frac{\sqrt{S}}{2}, 0, 0 \right) \quad (4.1)$$

and will find that the anomaly is a simple pole, of the Feynman integral, at $S = \infty$, which results from the combination of the asymptotic pinching of mass-shell propagator poles (those hatched in Fig. 2) with the large momentum behavior of off-shell propagators. The on-shell propagators will be used to carry out longitudinal momentum integrations and

produce a reduction to the transverse momentum integral of Fig. 1. The large momentum behavior will be a combination of the transverse momentum dependence of the exchanged propagators and the internal loop momentum dependence of the propagators in the left and right side triangle diagrams corresponding to Fig. 3.

A. Internal momenta and the quark mass-shell conditions

We consider, first, the left-hand box subgraph that appears in Fig. 5. As shown, we direct P_+ along the left-most quark line and use the k'_- integration to put this line on shell, i.e.,

$$\int dk'_- \frac{i \gamma(P_+ + \dots)}{(k'_- + p'_-) P_+ + i \epsilon + \dots} \xrightarrow{P_+ \rightarrow \infty} \pi \gamma_- + \dots \quad (4.2)$$

By using k'_- for this purpose, we keep the p' integration as a four-dimensional integral that we can anticipate will have an anomaly contribution from the large momentum region, as $P_+ \rightarrow \infty$.

Using the k'_- integration as in Eq. (4.2) has, however, the disadvantage that it introduces additional p' dependence into two of the propagators forming the triangle diagram. Consequently the triangle diagram no longer has the elementary structure known to generate the anomaly. We will avoid this problem by considering only a limited part of the p' integration, i.e., we consider the region where the components of p' have the order of magnitude

$$|p'_+| \sim \epsilon S^{1/2} \ll P_+, \quad p'^2_{\perp} \sim \epsilon M S^{1/2} \ll M P_+, \quad |p'_-| \sim \epsilon M, \quad (4.3)$$

where ϵ is small, but finite. As we will see, this will allow us to ignore the k'_- dependence of triangle diagram propagators while simultaneously keeping only the transverse momentum dependence of the exchanged propagators and also allowing the anomaly spin structure to emerge as a large k_{\perp} approximation.

We will use powers of ϵ as a simple way to impose inequalities amongst momenta that we could equally well impose more abstractly. We will integrate over a range of momenta having the given order of magnitude. Since we are only interested in showing that an anomaly power enhancement occurs, and will make no attempt to determine the coefficient multiplying it, the use of powers of ϵ will be sufficient to carry through our arguments. Note that as we explicitly discuss later, if we allowed p'_- to be slightly larger, i.e., $|p'_-| \sim M$, a Lorentz transformation on Eq. (4.3) would give all components the same order of magnitude, i.e., $p'_i \sim (\epsilon M)^{1/2} S^{1/4}$. In this case, however, the approximations we make in the following would be more marginal, and more discussion of their justification would be required. For simplicity, therefore, we keep $|p'_-| \sim \epsilon M$, although we believe the full anomaly generating region includes $|p'_-| \sim M$.

If k'_{\perp} is also large, but small compared to p'_{\perp} , say

$$k'^2_{\perp} \sim \epsilon^{3/2} M S^{1/2} \ll p'^2_{\perp} \quad (4.4)$$

The parallel discussion of the on-shell contribution of the right-side internal vector meson will give a corresponding constraint on $|k_+|$. The two constraints, taken together with Eq. (4.9), imply that (as for the gluon) transverse momenta dominate the central quark and antiquark propagators. As we noted, ensuring that k_- remains finite, with Eq. (4.9) satisfied, provides part of the motivation for the initial choice of Eq. (4.3) as the p' integration region.

Note that, although we consider very large transverse momenta, because the vector mesons remain on shell the high-energy behavior we will find will be scaled by M^2 . Consequently, there is no possibility that it could be cancelled by the contribution of a Higgs particle. (That is, if the Higgs mechanism were used to generate the vector meson mass.)

$$\frac{\hat{\gamma}}{\hat{k}} G_L(k_\perp, k'_\perp) \frac{\hat{\gamma}^*}{\hat{k}^*} \sim \frac{\hat{\gamma}}{\hat{k}} \left(\int d^4 p' \frac{\hat{k} \hat{\gamma}^* (\hat{p}' + \hat{k}')^* \hat{\gamma} \gamma_- (\hat{p}' + \hat{k}') \hat{\gamma}^* \gamma_+ [\hat{p}']^* \hat{\gamma} \gamma_-}{(p' + k')^4 (p')^2} \frac{\hat{\gamma}^*}{M^2} \right) \frac{\hat{\gamma}^*}{\hat{k}^*} \quad (4.12)$$

with the integration region specified by Eq. (4.3).

With Eqs. (4.3)–(4.5) satisfied, we can make the approximations

$$\begin{aligned} |k'_+(p'_- + k'_-)| &\sim \epsilon^2 M^2, \\ |p'_+(p'_- + k'_-)| &\sim \epsilon^2 M S^{1/2}, \\ (p' + k')_\perp^2 &\sim [\epsilon + O(e^{5/4})] M S^{1/2} \end{aligned} \quad (4.13)$$

and so

$$(p' + k')^2 \sim (p' + k')_\perp^2. \quad (4.14)$$

Consequently, we can approximate Eq. (4.12) as (again ignoring an overall constant)

$$\begin{aligned} \frac{\hat{\gamma}}{\hat{k}} G_L(k_\perp, k'_\perp) \frac{\hat{\gamma}^*}{\hat{k}^*} \\ \sim \frac{\hat{\gamma}}{\hat{k}} \left(\int d^4 p' \frac{\hat{k} [\hat{p}']^*}{[p'_\perp + k'_\perp]^2 [2p'_+ p'_- - (p'_\perp)^2]} \frac{\gamma_-}{M^2} \right) \frac{\hat{\gamma}^*}{\hat{k}^*} \end{aligned} \quad (4.15)$$

with the integration region still specified by Eq. (4.3).

Because we have eliminated k'_- and k'_+ (which are functions of p' and p''), the amplitude (4.15) is (almost) that of a conventional triangle Feynman diagram—with local vertices. Achieving the elimination of k'_- and k'_+ from Eq. (4.15)

D. The internal quark numerator and the triangle amplitude

For the remaining components of Fig. 3 that we have not yet discussed, the largest contribution (that also gives the γ_- vertex as in Fig. 7) is obtained by taking the gluon coupling to be γ_+ and taking the remaining quark numerator to also be transverse. The chirality then feeds through the propagator as illustrated in Fig. 8.

Combining Figs. 6, 7, and 8, and using Eq. (4.10) we obtain an effective triangle diagram with the numerators and vertices shown in Fig. 9. In this figure we have also included the transverse quark and antiquark propagators ($\hat{\gamma}/\hat{k}$ and $\hat{\gamma}^*/\hat{k}^*$) that are external to the triangle diagram. The amplitude obtained from Fig. 9 is (apart from an overall constant that we neglect-involving a numerical factor, factors of π , and powers of the coupling constants)

was, as we remarked, part of the motivation for the initial restriction to the momentum region (4.3)–(4.5).

E. The anomaly contribution

Using Eq. (A4) we can write the numerator momentum factor of Eq. (4.15) as

$$\hat{k} [\hat{p}']^* = k_\perp \cdot p'_\perp + i k_\perp \times p'_\perp. \quad (4.16)$$

The first term is not special to a vector vertex fermion triangle diagram and is not related to the anomaly. We expect it to arise from (and to eventually be cancelled by) a variety of contributions to the complete transverse momentum couplings of Fig. 1. It is the second term in Eq. (4.16) that we expect to give an anomaly contribution. It's parity properties result directly from the product of an odd number of quark numerators and so we anticipate that it can only be cancelled by effective triangle diagrams that contain three quark propagators.

Keeping just the second term in Eq. (4.15) gives, for the integral within the brackets (apart from the factor of γ_-/M^2)

$$\int d p'_+ d p'_- \int d^2 p'_\perp \frac{i k_\perp \times p'_\perp}{[p'_\perp + k'_\perp]^2 [2p'_+ p'_- - (p'_\perp)^2]}. \quad (4.17)$$

To carry out the angular integration for p'_\perp we choose coordinates (p'_2, p'_3) such that k'_\perp lies along the two axis. In this case,

$$p'_\perp k'_\perp = |p'_\perp| |k'_\perp| \cos \phi, \quad p'_\perp \times k'_\perp = |p'_\perp| (k_3 \cos \phi - k_2 \sin \phi), \quad (4.18)$$

where k_2 and k_3 are projections of k_\perp along and perpendicular to k'_\perp . We can, therefore, write

$$\begin{aligned} & \int dp'_+ dp'_- \int \frac{d(p'_\perp)^2}{[2p'_+ p'_- - (p'_\perp)^2]} \frac{k_\perp \times p'_\perp}{[p'_\perp + k'_\perp]^2} \\ &= \int dp'_+ dp'_- \int \frac{d(p'_\perp)^2}{[2p'_+ p'_- - (p'_\perp)^2]} \\ & \quad \times \int_0^{2\pi} d\phi \frac{|p'_\perp| (k_3 \cos \phi - k_2 \sin \phi)}{[(p'_\perp)^2 + (k'_\perp)^2 + 2|p'_\perp| |k'_\perp| \cos \phi]}. \end{aligned} \quad (4.19)$$

Using

$$\int_0^{2\pi} d\phi \frac{\sin \phi}{a + b \cos \phi} = -\frac{1}{b} [a + b \cos \phi]_0^{2\pi} = 0 \quad (4.20)$$

and

$$\begin{aligned} \int_0^{2\pi} d\phi \frac{\cos \phi}{a + b \cos \phi} &\sim \frac{1}{a} \int_0^{2\pi} d\phi \cos \phi - \frac{b}{a^2} \int_0^{2\pi} d\phi \cos^2 \phi \\ &+ O\left(\left[\frac{b^2}{a^3}\right]\right) \sim 0 - \frac{\pi b}{a^2} + O\left(\left[\frac{b^2}{a^3}\right]\right) \end{aligned} \quad (4.21)$$

we obtain

$$\int d\phi \frac{k_\perp \times p'_\perp}{[p'_\perp + k'_\perp]^2} \sim \frac{k_3 |k'_\perp|}{p'^2_\perp} \sim \frac{k_\perp \times k'_\perp}{p'^2_\perp}. \quad (4.22)$$

Equation (4.19) gives, therefore,

$$\begin{aligned} & k_\perp \times k'_\perp \int_{p'^2_\perp \sim \epsilon M \sqrt{S}} \frac{d(p'_\perp)^2}{(p'_\perp)^2} \\ & \quad \times \int_{|p'_+| \sim \epsilon \sqrt{S}, |p'_-| \sim \epsilon M} \frac{dp'_+ dp'_-}{[2p'_+ p'_- - (p'_\perp)^2]}. \end{aligned} \quad (4.23)$$

If we change variables to

$$\sqrt{S}x = p'^2_\perp, \quad \sqrt{S}y = p'_+ \quad (4.24)$$

we obtain

$$\begin{aligned} & \int_{p'^2_\perp \sim \epsilon M \sqrt{S}} \frac{d(p'_\perp)^2}{(p'_\perp)^2} \int_{|p'_+| \sim \epsilon \sqrt{S}, |p'_-| \sim \epsilon M} \frac{dp'_+ dp'_-}{[2p'_+ p'_- - (p'_\perp)^2]} \\ &= \int_{x \sim \epsilon M} \frac{dx}{x} \int_{|y| \sim \epsilon, |p'_-| \sim \epsilon M} \frac{dy dp'_-}{[2yp'_- - x]} \end{aligned} \quad (4.25)$$

which is clearly a constant that we do not need to evaluate.

Equation (4.23) is sufficient to conclude that the integration region on which we have focused gives, for Eq. (4.15), the behavior

$$\sim \frac{\hat{\gamma}^* \left(\frac{(k_\perp \times k'_\perp) \gamma_-}{M^2} \right) \hat{\gamma}}{\hat{k}^*}. \quad (4.26)$$

F. Behavior of the full amplitude

It is straightforward to obtain the behavior of the full amplitude that results from combining Eq. (4.26) with the corresponding contribution from the right-side box graph in Fig. 5. As we have discussed above, the internal mass-shell conditions determine that the longitudinal momenta in the central propagators of Fig. 5 can be neglected. As a result the k'_\perp and k_\perp loop integrations produce, as anticipated, a transverse momentum integral of the form of Eq. (3.1) which we write, in complex γ -matrix notation, as

$$\begin{aligned} & \int \frac{d^2 k'_\perp}{k'^2_\perp} \int d^2 k_\perp \text{Tr} \left\{ \frac{\hat{\gamma}}{\hat{k}} G_L(k_\perp, k'_\perp) \frac{\hat{\gamma}^*}{\hat{k}^*} G_R(k_\perp, k'_\perp) \right\} \\ & \sim \int \frac{d^2 k'_\perp}{k'^2_\perp} \int d^2 k_\perp \left(\frac{k_\perp \times k'_\perp}{M^2} \right)^2 \frac{\text{Tr} \{ \gamma_- \hat{\gamma}^* \gamma_+ \hat{\gamma} \}}{\hat{k} \hat{k}^*} \\ & \sim \int \frac{d^2 k'_\perp d^2 k_\perp}{k'^2_\perp k^2_\perp} \left(\frac{k_2 k'_3 - k_3 k'_2}{M^2} \right)^2. \end{aligned} \quad (4.27)$$

Since the foregoing analysis assumes that both Eqs. (4.4) and (4.9) hold, it follows that both k'^2_\perp and k^2_\perp can be integrated over a range of values, that are $O(MS^{1/2})$ without either the approximations that we have made breaking down or the transverse momentum approximation to the gluon and quark propagators being invalidated. Therefore, we obtain a contribution from Eq. (4.27) of the form

$$\begin{aligned} & \int \frac{d^2 k'_\perp}{k'^2_\perp} \int d^2 k_\perp \text{Tr} \left\{ \frac{\hat{\gamma}}{\hat{k}} G_L(k_\perp, k'_\perp) \frac{\hat{\gamma}^*}{\hat{k}^*} G_R(k_\perp, k'_\perp) \right\} \\ & \sim \frac{1}{M^4} \int_{O(MS^{1/2})} d(k'^2_\perp) \int_{O(MS^{1/2})} d(k^2_\perp) \sim \frac{S}{M^2}. \end{aligned} \quad (4.28)$$

[Note that, because the anomaly contribution to $G_L(k_\perp, k'_\perp)$ is linear in k'_\perp , if it is combined with a $G_R(k_\perp, k'_\perp)$ that does not have this contribution then integration over k'_\perp will give a cancellation of the enhancement effect. This is why we have considered a diagram which gives anomaly contributions to both G_L and G_R .]

As we noted above, because two fermion exchange is involved, we would have expected the amplitude to increase only as some power of $\ln S$. However, we have now shown that the kinematic region of Fig. 5 that we have isolated actually produces a power enhancement of the expected high

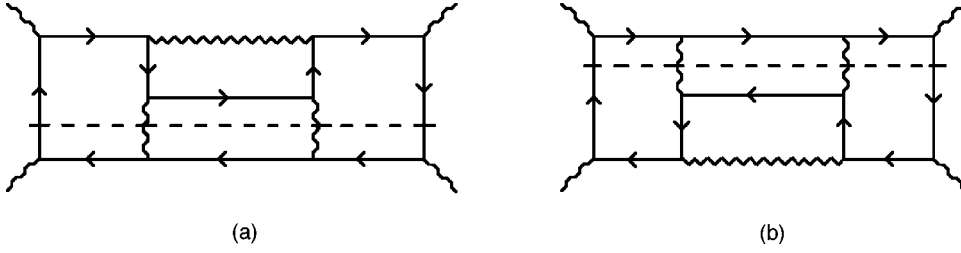


FIG. 10. Unitarity cuts of (a) the diagram of Fig. 2 and (b) a related diagram.

energy behavior. As we will see in the next section, there are no accompanying logarithms in this lowest-order appearance of the anomaly.

Clearly, if a fixed transverse momentum cutoff is imposed, i.e.,

$$k'_\perp, k_\perp^2 < \lambda_\perp \quad (4.29)$$

then there will be no contribution of the form (4.28) when S is sufficiently large. Therefore, a transverse cutoff eliminates the enhancement effect and restores the normal behavior expected for two fermion exchange. However, as we discuss at greater length in Sec. VII, a transverse cutoff violates gauge invariance Ward identities in a way that replaces the anomaly enhancement by transverse momentum infrared divergences.

G. Comparison with the axial vector vertex anomaly

To see the relationship between the anomaly amplitude (4.26) that we have found and the familiar axial vector anomaly we proceed as follows. First we change variables from p' to q , where

$$q_+ = \frac{p'_+}{\Lambda}, \quad q_- = \Lambda p'_-, \quad q_\perp = p'_\perp, \quad \Lambda = \left(\frac{\epsilon}{M}\right)^{1/2} S^{1/4}. \quad (4.30)$$

If we also extend the integration region for p'_- to $p'_- \sim M$ (which, as we have already noted, would not significantly alter the above analysis) then Eq. (4.15) becomes (moving the γ_-/M^2 outside of the brackets)

$$\frac{\hat{\gamma}}{\hat{k}} \left(\int_{|q_j| \sim (\epsilon M)^{1/2} S^{1/4}} d^4 q_j \frac{\hat{k} \hat{q}^*}{[q_\perp + k'_\perp]^2 [2q_+ + q_- - q_\perp^2]} \right) \frac{\gamma_- \hat{\gamma}^*}{M^2 \hat{k}^*}, \quad (4.31)$$

where, as indicated the range of integration is now the same for all components of q . In the limit $S \rightarrow \infty$, the integration is over a four-dimensional large momentum region and, for-

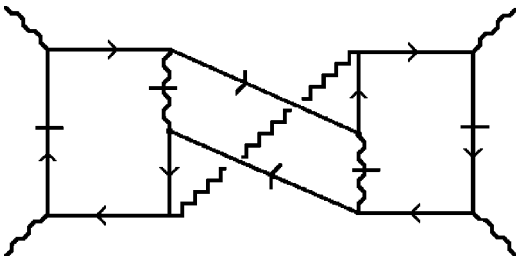


FIG. 11. A twisted diagram.

mally, the integral is linearly divergent. Also, a product of three orthogonal γ matrices is present—although there is no trace involved. Consequently, it is natural to expect a large momentum contribution of the form associated with the triangle anomaly.

The strictly infinite momentum region contribution to Eq. (4.31) is

$$\sim \frac{\hat{\gamma}}{\hat{k}} \left(\int dq_+ dq_- \int d^2 q_\perp \left[\frac{k_\perp \times q_\perp}{q_\perp^2} \right] \frac{1}{[2q_+ + q_- - q_\perp^2]} \right) \times \frac{\gamma_- \hat{\gamma}^*}{M^2 \hat{k}^*}. \quad (4.32)$$

which, integrating by parts with respect to q_\perp^2 , we can rewrite as

$$\sim \frac{\hat{\gamma}}{\hat{k}} \left(\int dq_+ dq_- \int d^2 q_\perp \frac{k_\perp \times q_\perp}{[2q_+ + q_- - q_\perp^2]^2} \right) \frac{\gamma_- \hat{\gamma}^*}{M^2 \hat{k}^*} \quad (4.33)$$

and, with a further integration by parts, as

$$\sim \frac{\hat{\gamma}}{\hat{k}} \left(\int dq_+ dq_- \int d^2 q_\perp \frac{q_\perp^2 [k_\perp \times q_\perp]}{[2q_+ + q_- - q_\perp^2]^3} \right) \frac{\gamma_- \hat{\gamma}^*}{M^2 \hat{k}^*}. \quad (4.34)$$

Undoing the γ -matrix removal involved in going from Eqs. (4.12)–(4.15) (or, equivalently, inserting γ matrices using $2 = \gamma_+ \gamma_- + \gamma_- \gamma_+ = \hat{\gamma} \hat{\gamma}^* + \hat{\gamma}^* \hat{\gamma}$) we can rewrite Eq. (4.34) as

$$\sim \hat{\gamma} \left(\int_{|q_i| \gg O(M)} d^4 q \frac{\hat{\gamma}^* [\hat{q}^* \hat{\gamma}] \gamma_- [\hat{q} \hat{\gamma}^*] \gamma_+ [\hat{q}^* \hat{\gamma}]}{[q^2]^3} \right) \frac{\gamma_- \hat{\gamma}^*}{M^2 \hat{k}^*} \\ \sim \hat{\gamma} \left(\int_{|q_i| \gg O(M)} d^4 q \frac{\tilde{\gamma}^* \not{q}_\perp (1 - \gamma_5) \gamma_- \not{q}_\perp \gamma_+ \not{q}_\perp}{[q^2]^3} \right) \frac{\gamma_- \hat{\gamma}^*}{M^2 \hat{k}^*}. \quad (4.35)$$

We recognize the integral, within the brackets, of Eq. (4.35) as a left-handed transverse propagator contribution to a tensor component of the standard large momentum anomaly integral (apart from the feature that there is no trace of the γ matrices involved). Therefore, we could anticipate

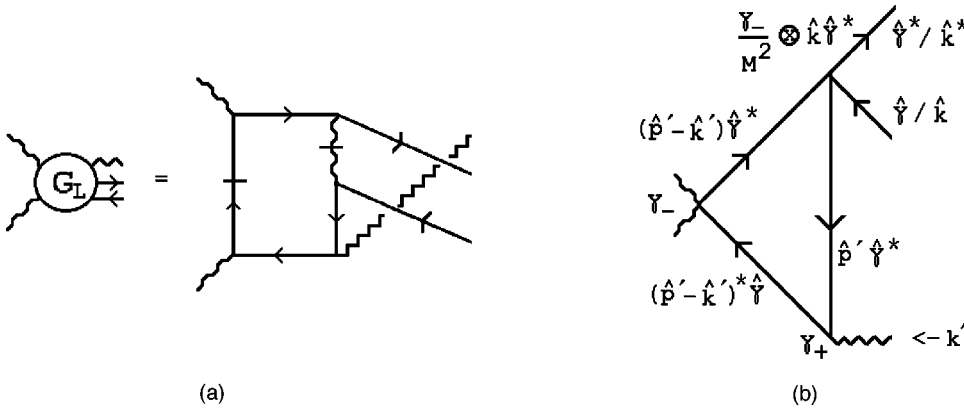


FIG. 12. (a) The G_L generated by Fig. 11. (b) The effective triangle diagram.

Eq. (4.26) directly from the familiar anomaly contribution to a three current vertex $T_{\mu\alpha\beta}(k_1, k_2)$ —the notation is that of Fig. 54. In our case,

$$k_1 = -k_2 = k'_\perp \tag{4.36}$$

and if we consider the decomposition into invariant amplitudes (C1), Eq. (4.26) corresponds to the contribution of the first two terms, which are linear in k_1 and k_2 .

It is very well known that in the three-current vertex the ambiguity of the ultraviolet anomaly contribution is determined by vector current Ward identities that relate the anomaly contribution to infrared triangle diagram contributions. In our case, we anticipate that there will be a (Reggeized) gluon Ward identity which similarly determines the coefficient of the anomaly contribution we have found. We discuss this point further in Sec. V. Note, however, that, in the special momentum configuration (4.36), all the other terms in Eq. (C1) vanish—if there are no infrared divergences to consider. Therefore, in the lowest-order graphs we are discussing, the ultraviolet anomaly contributions we are discussing cannot be cancelled by the contribution of infrared transverse momentum regions.

V. NONCANCELLATION OF THE ANOMALY

In this section we consider other diagrams that are also $O(\alpha_s)$ and similarly have anomaly enhancements that might produce an overall cancellation.

A. Reality of the anomaly amplitude

It is significant that the anomaly amplitude we have found, although calculated with internal lines on shell, is real. Indeed there is no evidence, in the amplitude, of either the s -channel or the t -channel intermediate states that are present in the diagram from which it was calculated. At first

sight this seems paradoxical since it would appear that the analysis of Fig. 2, in the previous section, can be viewed as the calculation of an s -channel discontinuity—via the unitarity cut corresponding to the dashed line in Fig. 10(a).

The tree amplitude that appears below the cut is integrated with the one loop amplitude that appears above the cut. That the calculation can be related to the evaluation of a discontinuity immediately justifies, in fact, our choice of lines to place on shell.

That there is ultimately no discontinuity associated with the anomaly is due to a second discontinuity contribution from the unitarity cut of a closely related graph shown in Fig. 10(b). Clearly Fig. 10(b) is so similar to Fig. 10(a) that our analysis carries over directly. In both cases, the intermediate state integration over k_\perp produces an imaginary contribution of $i|S|^{1/2}$. However, the k'_\perp integration, that also gives a factor of $i|S|^{1/2}$, is part of the integration within the loop amplitude.

If we formulate the above analysis as a unitarity calculation then the amplitude on one side of the cut must be complex conjugated. As a result, the loop amplitude will have the opposite sign in the contributions from Figs. 10(a) and 10(b) and since all other parts of the diagrams contribute identically, adding the two will give a factor of

$$(2\pi)^4 ([i|S|^{1/2}][i|S|^{1/2}] + [i|S|^{1/2}][-i|S|^{1/2}]) = 0. \tag{5.1}$$

Alternatively, if we calculate the contribution of the two diagrams as that of amplitudes then the loop amplitude will have the same sign in both cases and Eq. (5.1) will be replaced by

$$(\pi)^4 ([i|S|^{1/2}][i|S|^{1/2}] + [i|S|^{1/2}][i|S|^{1/2}]) = 2\pi^4 S. \tag{5.2}$$

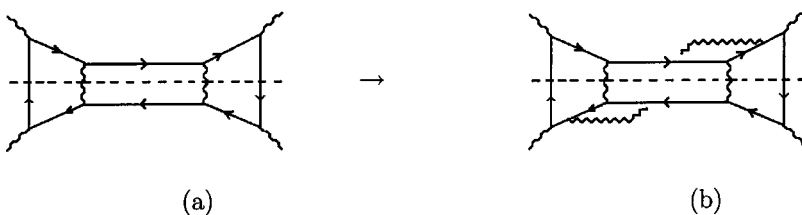


FIG. 13. Addition of an exchanged gluon to a cut amplitude.

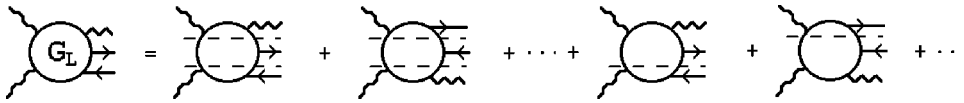


FIG. 14. Representation of the double dispersion relation for G_L .

which will, indeed, give a real amplitude. The contribution of Fig. 10(b) simply doubles that of Fig. 10(a). The absence of a discontinuity implies that, as we anticipated earlier, there are no additional logarithms accompanying the power enhancement due to the anomaly. As we stated in the last section, the anomaly is a simple pole at $S = \infty$ which results from the combination of the asymptotic pinching of the mass-shell poles of the hatched propagators with the large momentum behavior of the unhatched propagators.

B. Another anomaly generating diagram

The diagram of Fig. 10(b) is obtained from that of Fig. 10(a) by simultaneously “twisting” both the left and right-side box diagrams. For much of our discussion (including the addition of extra gluons in the next section) we will keep the right-side of the diagrams we consider, and therefore the corresponding G_R , fixed and discuss anomaly amplitudes entirely in terms of possible left-side contributions to G_L . In the simple case of the one gluon diagrams that we are presently discussing, the right-side coupling will be that of Fig. 2 [or Fig. 10(a)] and it will be clear that, as in the above discussion, diagrams with the right-side coupling of Fig. 10(b) simply give parallel contributions. However, when we consider infrared cancellations in the next section, it will be essential to also consider all contributions to G_R .

Consider, next, the diagram shown in Fig. 11 that is obtained from that of Fig. 2 by twisting the left half of the diagram relative to the right half. By a similar application of the above analysis, which puts on shell the hatched lines shown in Fig. 11, the transverse momentum diagram of Fig. 1 will again be generated. The G_L shown in Fig. 12(a), obtained from the left part of Fig. 11, contains the effective triangle diagram shown in Fig. 12(b).

A very similar expression to Eq. (4.26) will clearly be obtained. The differences in the analysis can be summarized as follows.

- (i) The analogue of Eq. (4.12) gives Eq. (4.15) but with $\hat{k}[\hat{p}']^* \rightarrow \hat{k}^* \hat{p}'$ which leads to $k_{\perp} \times p'_{\perp} \rightarrow -k_{\perp} \times p'_{\perp}$ in Eq. (4.17) and the following.
- (ii) A second change of sign arises from $k'_{\perp} \rightarrow -k'_{\perp}$ in Eq. (4.15).

The net result is that an identical anomaly contribution, to that obtained from Fig. 2, is obtained from the diagram of Fig. 11.

The lines placed on shell, asymptotically, in Fig. 11 do not correspond to a simple cut of the diagram, as was the case for Fig. 2. However, Fig. 11 can also be represented as in Fig. 13(b), i.e., as an exchanged gluon attached to the off-shell lines of the cut amplitude of Fig. 13(a). The exchanged gluon has transverse momentum much less than the off-shell quark or antiquark to which it couples in the large momentum p' and p'' regions which generate the anomaly. Consequently, it does not interfere (kinematically) with either the quark-antiquark scattering process, or the asymptotic placing

on shell of the left side fast quark and the right side antiquark. Therefore, the justification for the choice of lines placed on shell is closely related to the existence of the asymptotic physical region discontinuity of Fig. 13(a). The asymptotic pinching of the particle poles that gives the discontinuity in Fig. 13(a), together with the large momentum behavior of the uncut propagators, is responsible for the pole at infinite momentum in Fig. 13(b) that corresponds to the anomaly.

A second, essential, point related to the choice of on-shell lines is the following. According to multi-Regge theory, the coupling G_L can be evaluated by a double dispersion relation, represented schematically in Fig. 14—where the cuts represent the discontinuities involved. As a consequence, G_L can be expressed as a sum over dispersion integrals which give amplitudes corresponding to all possible double discontinuities plus, possibly but not necessarily, (generalized) subtraction terms containing just single discontinuities. The anomaly contributions we have found are, in fact, generalized subtraction terms and the contributions of Figs. 3 and 12, respectively, correspond to the two single discontinuity terms shown explicitly in Fig. 14. However, since we are evaluating an amplitude, and not a discontinuity, to have a contribution with on-shell lines corresponding to particular single discontinuities of G_L and G_R , these discontinuities must be present in the asymptotic kinematic region we are considering. In fact, the discontinuity line in Fig. 13(b) can be regarded as representing the combination of the relevant discontinuities of G_L and G_R .

C. Possible cancellation mechanisms

If we consider just contributions to the transverse momentum diagram of Fig. 1, then Fig. 11 is the only diagram which contributes [via the coupling of Fig. 6(a)] to the same helicity amplitude as Fig. 2 and which generates an appropriate effective triangle diagram, apart from the diagram obtained by similarly twisting Fig. 10(b). We can not twist just the quark-antiquark state since this would reverse the direction of the quark arrow along the fast quark line, requiring a change of the external helicity to obtain a coupling. We conclude, therefore, that the full anomaly contribution to G_L is obtained by adding the two effective triangle diagrams of Fig. 15. Therefore, within the transverse momentum diagram

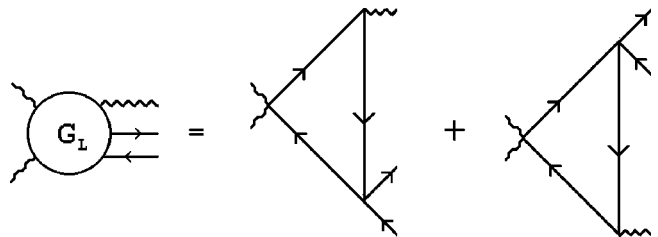


FIG. 15. The two effective triangle diagrams generating the anomaly.

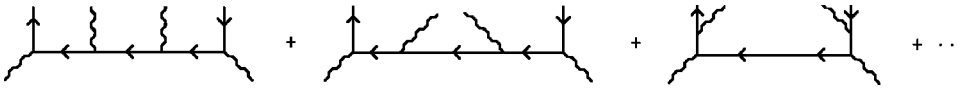


FIG. 16. Tree diagrams contributing to electroweak ward identities.

of Fig. 1, the anomaly enhancement does not cancel.

It is natural, however, to expect that there will be further cancellations. As we emphasized in the Introduction, because longitudinal vector meson contributions are involved, it is important to look for all possible cancellation mechanisms that could be associated with an underlying gauge invariance. In particular, because the left-side quark and right-side antiquark are asymptotically on shell, we must consider whether asymptotic electroweak Ward identities could lead to the cancellation of the vector meson numerator contributions that are producing the anomaly enhancement.

There are two obvious Ward identity related cancellations that we should consider. First, we consider the tree diagram that appears in the lower half of Fig. 10(a). At finite momentum, if the intermediate state quark and antiquark are strictly on shell, there will be Ward identities involving this diagram and all other diagrams obtained by attaching the internal vector meson lines at all possible points. Examples of such diagrams, together with the initial diagram, are shown in Fig. 16. In fact, because the intermediate state quark and antiquark are only asymptotically on shell, we might expect that only the vector meson numerator components that are parallel to the asymptotic light-cone quark and antiquark momenta must decouple. This decoupling has already appeared in the analysis of Sec. IV C.

In Appendix D we study in detail the Ward identity cancellations associated with the tree diagrams of Fig. 16. The essential part of the first diagram in Fig. 16 is, indeed, directly cancelled by the contribution of the second diagram, which corresponds to the Feynman diagram shown in Fig. 17. However, the anomaly enhanced amplitude produced by Fig. 17 appears to not be representable as a transverse momentum diagram divergence.

More surprisingly, perhaps, essentially the same anomaly enhanced amplitude then reappears via the contribution of the third diagram in Fig. 16, which corresponds to the Feynman diagram shown in Fig. 18. This is a diagram that would normally be neglected because off-shell propagators are carrying large light-cone momenta.

In a sense, therefore, nothing is gained by implementing the Ward identity cancellations. However, after this implementation it is apparent that the lack of anomaly cancellation

is entirely due to the asymptotic nature of the placing on shell of the quark and antiquark lines. Also, when the Ward identity cancellations are carried out several diagrams are included, in addition to Fig. 18, that would normally be considered nonleading. This makes it clear that there is a general phenomenon of superficially nonleading high-energy behavior contributing to the leading behavior because of large transverse momentum divergences.

There is also a second Ward identity, involving the top part of Fig. 10(a) and other loop diagrams, some of which are shown in Fig. 19, that might be expected to lead to the decoupling of the top $\gamma_{-p'_+}$ vertex in Fig. 7, together with the corresponding $\gamma_{+p''_-}$ right-side vertex. These vertices are crucially important for our analysis. However, in this case it is the intervention of the asymptotic anomaly that invalidates the potential asymptotic Ward identities and, self-consistently, prevents the decoupling of the vector meson vertices that are involved.

In conclusion, we can say that there is no cancellation of the transverse momentum coupling effective triangle diagram anomaly by another diagram with a similar anomaly. There may very well be a cancellation outside of the transverse momentum diagram formalism. However, in this paper at least, we will not pursue this possibility any further.

D. The same helicity scattering amplitude

To obtain an anomaly amplitude for the scattering of vector mesons which both have helicity $\lambda = +1$ we include the left side coupling of Fig. 6(b) within a diagram that otherwise is the same as Fig. 2 or Fig. 11. The result is the two diagrams shown in Fig. 20. When displayed in the first form, it is clear that the only difference between these diagrams and, respectively, Figs. 2 and 11 is that along the left-most vertical line $P_+ \rightarrow -P_+$. Therefore, if we evaluate the diagrams with the sign of P_+ reversed, corresponding to a cross-channel physical region, the appropriate on-shell configurations will be present. The diagrams will be kinematically identical, respectively, to Figs. 2 and 11 and will give identical anomaly contributions, but with $S \rightarrow -S$.

The second form for the diagrams displayed in Fig. 20 is more transparent for discussing symmetry properties of the intermediate state. In particular, in this form, it is clear that Fig. 20(b) can be obtained from Fig. 2 by twisting the quark-

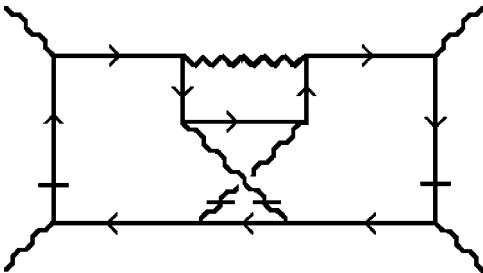


FIG. 17. A Feynman diagram with a canceling anomaly contribution.

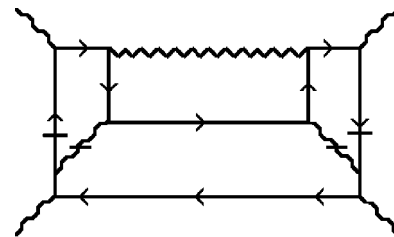


FIG. 18. The Feynman diagram corresponding to the third tree diagram in Fig. 16.

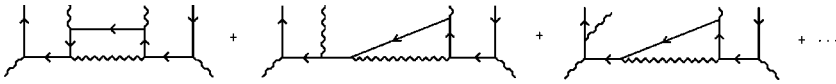


FIG. 19. Loop diagrams contributing to electroweak Ward identities.

antiquark intermediate state (together with the necessary redirection of the quark arrow in the left part of the diagram). Figure 20(a) can similarly be obtained from Fig. 11.

E. Cancellation in a vector theory

If the vector mesons we are considering had a vector coupling, rather than a left-handed coupling, to quarks, then the diagrams of Fig. 16 would appear also in the opposite sign helicity amplitude but with $(1 + \gamma_5)$ couplings replacing the $(1 - \gamma_5)$ couplings in Fig. 6(b). In this case, after the use of Eq. (A15), the relative minus sign discussed in the previous subsection (resulting from $S \rightarrow -S$) produces a cancellation between the anomaly contributions from Figs. 2 and 20(a). Similarly, the contributions from Figs. 11 and 20(b) cancel. In a vector theory, this cancellation of right and left-handed coupling contributions would persist, even as we add more gluons as discussed in the next section.

F. The even signature amplitude

To form signed scattering amplitudes we should add to, or subtract from, a particular helicity amplitude the amplitude obtained by a CPT transformation of one scattering state relative to the other. Therefore, if A_{-+} and A_{++} are the opposite sign and same sign amplitudes we have discussed,

$$A^\pm(P_+, P_-) = A_{-+}(P_+, P_-) \pm A_{++}(-P_+, P_-) \tag{5.3}$$

is an even-odd signature amplitude. This implies that the anomaly amplitudes arising from Figs. 2 and 20(a) are added in the even signature amplitude and subtracted in the odd signature amplitude [as are the anomaly amplitudes arising from Figs. 11 and Fig. 20(b)]. Therefore, the anomaly cancels in the odd signature amplitude and is present only in the even signature amplitude. This will continue to be the case as we add more gluons in the next section. It is directly related, via a generalization of the discussion of the previous two subsections, to the cancellation in a vector theory.

G. C and P properties of the transverse momentum state

Since the intermediate state in Fig. 1 is completely transverse (or, equivalently, is a t -channel intermediate state) the T part of the CPT transformation, defining the signature of an amplitude, has no effect on it. Therefore, we should be able to relate signature directly to the CP properties of the transverse momentum state.

The parity transformation reverses the transverse momentum of the gluon and so, because of the coupling (4.26), simply gives a minus sign. Without a color factor, the charge conjugation transformation also gives just a minus sign. Therefore, the gluon component of the intermediate state is even under CP . For quarks the left-handed coupling violates both P and C . As a result, the quark-antiquark intermediate state only has simple transformation properties under the combined CP transformation. Charge conjugation transforms a quark (antiquark) to the corresponding antiquark (quark), with the same helicity (opposite chirality). The parity part of the CP transformation then reverses the helicities. In our case, the quark and antiquark have opposite helicities and so they will be simply interchanged by the CP transformation. Individually, the diagrams we are discussing do not have simple symmetry properties with respect to quark/antiquark interchange. Not surprisingly, however, the full set of anomaly contributions in the even signature amplitude does have such a property.

With the four diagrams 2, 11, 20(a), and 20(b), added in the even signature amplitude, it is clear (using the second display form in Fig. 20) that the left-side coupling is symmetric, diagrammatically, with respect to the interchange of the quark and antiquark. The interchange relates Fig. 2 to Fig. 20(b) and Fig. 11 to Fig. 20(a). In addition to the reversal of the quark line, the contribution of Fig. 20(b) to the even signature amplitude differs kinematically from that of Fig. 2 in two ways that produce canceling sign changes. First, $k_\perp \rightarrow -k_\perp$ and, secondly, the effect in the k'_\perp integration of $P_+ \rightarrow -P_+$ resulting from the definition of the even signature amplitude. Therefore, in this amplitude, the quark-antiquark intermediate state is even under CP . Since the gluon state is also even under CP , the full transverse momen-

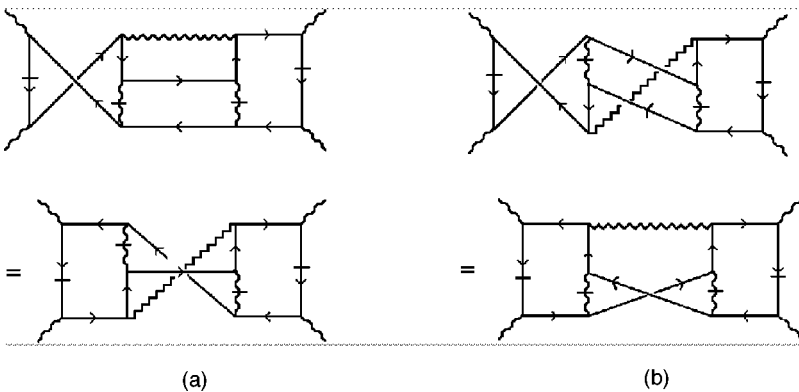


FIG. 20. The scattering of same helicity vector mesons.

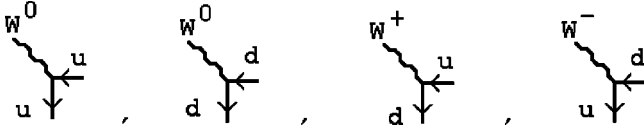


FIG. 21. Vector meson and quark vertices.

tum state is indeed even under CP , as it should be.

Note that the full even signature amplitude will contain, in addition to the four diagrams of Figs. 2, 11, 20(a), and 20(b), the four related diagrams obtained by substituting the right side of Fig. 10(b) for that of Fig. 10(a). In effect, in this second set of diagrams the twists are made on G_R that are made on G_L in the first set of diagrams. Each set of twists is sufficient to give an intermediate state with the appropriate CP property. As a result, the discussion of each set of four diagrams can be made separately and is directly parallel. In higher orders it will sometimes be necessary to consider both sets of twists together to obtain an intermediate state with the right CP property.

VI. COLOR FACTORS AND MORE GLUONS

We begin with a discussion of $SU(2)$ flavor that will, essentially, allow us to ignore it in the following.

A. $SU(2)$ flavor

The $SU(2)$ flavor symmetry will play only a minimal role in our discussion and we will introduce it in a very elementary manner. We consider the exchange of a quark-antiquark $\{I=1, I_z=0\}$ state that, in the standard model, would carry the quantum numbers of the π^0 . Identifying W^\pm, W^0 with the $\{I=1, I_z=\pm, 0\}$ vector mesons and identifying u, d with the $\{I=1/2, I_z=\pm 1/2\}$ quarks, we can add flavor quantum numbers to the discussion of the previous section by using the vector-meson-quark vertices of Fig. 21. The flavorless couplings of Fig. 6 are then replaced by the sums of couplings shown in Figs. 22(a) and 22(b) and the internal vector meson on-shell contributions are replaced by a similar sum.

We then add all the diagrams obtained with this set of couplings. The most important feature of these couplings is that they are symmetric with respect to $u \leftrightarrow d$ and that this symmetry is preserved by the internal vector meson exchange interactions. [It is also important for the CP properties of the diagrams we discuss that, in going from Fig. 22(a) to Fig. 22(b), left-handed quarks and right-handed antiquarks are interchanged, as was the case for Figs. 6(a) and 6(b).] Consequently, the addition of $SU(2)$ flavor factors will not produce any diagram cancellations and we can leave, as im-

PLICIT, the replacement of the couplings of Fig. 6 by those of Fig. 22.

B. Color factor diagrams and the one gluon color factor

$SU(3)$ color factors will also be relatively simple. In all the diagrams we discuss, there will be only one quark loop. There is no external color and so color is introduced into the quark loop only by the couplings to the internal gluons. Also, for the diagrams we consider, gluons will appear only as part of the exchanged transverse momentum state and will be attached within the corresponding G_L and G_R transverse momentum couplings. As a result, we can use a simple notation to describe color factors. We represent the quark loop as a rectangle, and attach gluons only to the vertical lines. The attachment of gluons to the left-side vertical line represents the order of attachment to the quark loop within the left-side transverse momentum coupling G_L , while the right-side vertical line similarly represents the order of attachment within G_R . For each gluon there is a color matrix λ_i at each attachment point. The full color factor is the trace of the product of the λ matrices taken around the loop, and then summed over $i=1, \dots, 8$ for each gluon. The notation is illustrated for various numbers of exchanged gluons in Fig. 23.

All of the diagrams discussed in the previous section contain just one gluon and have the same color factor. This is represented by Fig. 23(a) and is simply

$$\sum_i \text{Tr}\{\lambda_i^2\}. \quad (6.1)$$

Since all diagrams have the same color factor (and flavor factor) all of the discussion in the previous section is essentially unchanged, apart from the discussion of charge conjugation, which now has to include color charge conjugation.

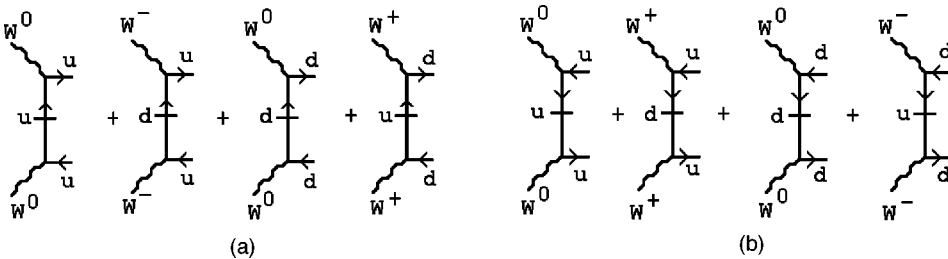
For a general gluon field with color matrix M_{ab} , color charge conjugation is defined as

$$M_{ab} \rightarrow [-M_{ab}]^T = -M_{ba}. \quad (6.2)$$

For the hermitian color matrix vertices λ_i

$$[-\lambda_i]^T = -[\lambda_i]^*, \quad (6.3)$$

where $[\dots]^*$ denotes complex conjugation. Therefore, in addition to the charge conjugation minus sign discussed in the last section, the coupling of the gluon to the quark line (within G_L , say) is complex conjugated. Correspondingly, for the quark-antiquark pair, in addition to the charge conjugation discussed in the previous section, quark-antiquark interchange gives

FIG. 22. Couplings with $SU(2)$ flavor quantum numbers.

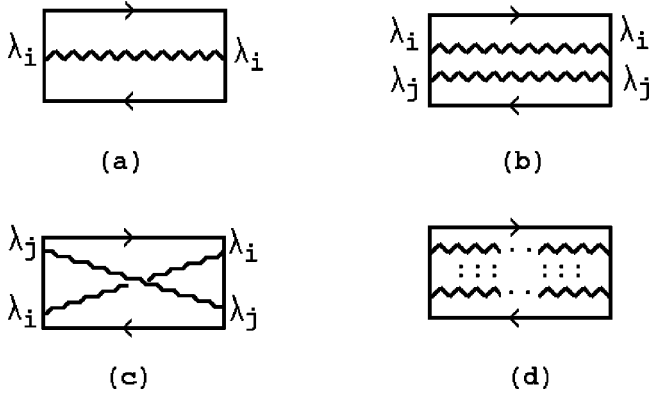


FIG. 23. Color factor diagrams.

$$[\lambda_i]^* \rightarrow [\lambda_i] \quad (6.4)$$

in Eq. (6.3). Since the parity transformation is unchanged, the full gluon plus quark/antiquark transverse momentum state remains even under CP when color charge conjugation is included.

C. The addition of a soft gluon

Next, we look for Feynman diagrams that contain two gluons and that also, potentially, contain the anomaly enhancement. We will assume that only one gluon is involved in the transverse momentum divergence and will consider two possibilities for the scale of the transverse momentum carried by the second gluon. It can either be “soft,” i.e., it carries a very small momentum k'' , with

$$|k''_{\perp}| \ll M \ll |k_{\perp}|, |k'_{\perp}| \leftrightarrow \text{“soft”} \quad (6.5)$$

or “finite,” i.e.,

$$|k''_{\perp}| \sim M \ll |k_{\perp}|, |k'_{\perp}| \leftrightarrow \text{“finite”}. \quad (6.6)$$

As we will see, in some diagrams soft gluon exchange is possible, in addition to the anomaly generation, while in others only finite gluon exchange is possible. In both cases, the second gluon will provide an important color factor. A soft gluon, however, will also produce an infrared divergence. Since the full transverse momentum state carries zero color, such divergences must cancel. This will help us to locate other diagrams generating the anomaly.

We consider the “soft” gluon case first and look for diagrams that contribute to the transverse momentum diagram of Fig. 24 which, as discussed further in Appendix B, would again be expected to contribute (formally) only at next-to-next-to-leading log. (Note that, when the anomaly is not

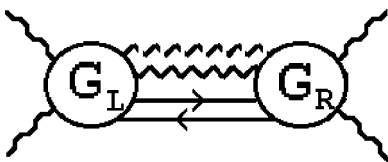


FIG. 24. The two gluon transverse momentum diagram. The broken line denotes a soft gluon.

present, this diagram again, potentially, includes a logarithmic transverse momentum divergence generating an additional energy logarithm.)

We begin with the addition of a soft gluon to the diagram of Fig. 2. The anomaly will appear in the same manner as before if, in the high-energy limit, an effective triangle diagram is generated as in Fig. 3, but with the additional gluon attached, via a point coupling, to one of the three vertices of the diagram. The required local coupling could appear, in principle, if k'' can be directed through an adjacent quark line which can be put on shell by the k''_{\perp} integration. If this line carries (predominantly) a large light-cone momentum then, in analogy with Eq. (4.2), the integration will produce couplings that are independent of k''_{\perp} . In Figs. 25(a), 25(b), and 25(c) we show how the extra gluon could be added to Figs. 6, 7, and 8, respectively, with the final γ matrices remaining the same as in Fig. 9.

In Fig. 25(c) the soft and hard gluon can be interchanged, whereas in Figs. 25(a) and 25(b) there is no ambiguity as to where the soft gluon has to be attached, if the γ -matrix structure is to remain the same.

For Fig. 25(a) we can, essentially, apply Eq. (4.2) directly. For the couplings of Figs. 25(b) and 25(c) there is, however, a problem if the extra gluon is soft and so carries only very small transverse momentum. In these cases, the propagator that has to be placed on shell by the k''_{\perp} integration is adjacent to an off-shell propagator that, in the anomaly configuration, is carrying very large transverse momentum (p'_{\perp}). In this case the mass-shell condition is

$$k''_{\perp} \sim \frac{(p'_{\perp} + k''_{\perp})^2}{p'_{\perp}} \sim \frac{\epsilon M \sqrt{S}}{\epsilon \sqrt{S}} \sim M \quad (6.7)$$

which cannot be satisfied with $k''_{\perp} \ll |k'_{\perp}| \ll M$. Therefore, if the vertex for the extra gluon is of the form of Fig. 25(b) or 25(c), in both the G_L and G_R couplings, then it cannot carry $|k''_{\perp}|^2 \ll M^2$.

Later, we will discuss potential contributions from vertices of the form of Figs. 25(b) and 25(c) when k'' is “finite,” i.e., $|k''_{\perp}|^2 \sim M^2$. For the moment, we consider only the vertex of Fig. 25(a). Generation of the corresponding triangle diagram of Fig. 26 and the full Feynman diagram, with the extra gluon attached in the same manner to both sides of Fig. 5, is shown in Fig. 27.

As illustrated, the lines put on shell correspond to making a double cut of the diagram. This corresponds to double discontinuity contributions to the G_L and G_R couplings. (These contributions are again generalized subtractions in that the full dispersion relations for G_L and G_R contain triple discontinuities.)

D. The two gluon anomaly amplitude

If k''_{\perp} is much smaller than any other transverse momentum in the diagram of Fig. 23, the only significant k''_{\perp} dependence will be in the k'' propagator. Hence, the k''_{\perp} integration can be factored out from the remaining integrations and, before the inclusion of any color factor, the diagram of Fig. 23

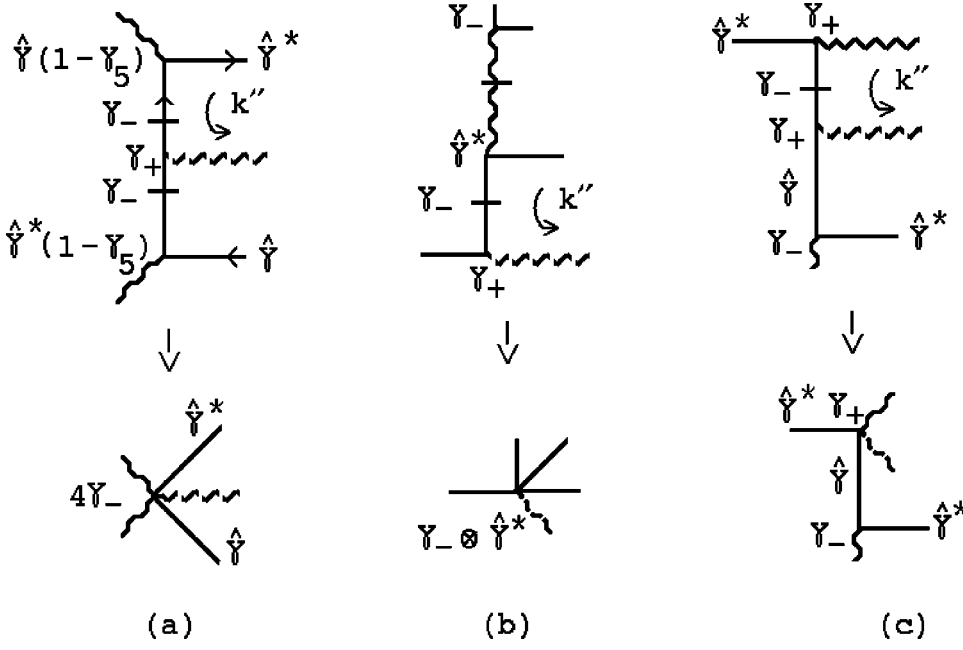


FIG. 25. Adding a gluon to the vertices of (a) Fig. 6, (b) Fig. 7, and (c) Fig. 8.

gives, via the reduction of Figs. 25(a) and 26, a high-energy anomaly enhanced amplitude of the form

$$\begin{aligned}
 & \int^{|k_{\perp}''| \ll M} \frac{d^2 k_{\perp}''}{k_{\perp}''^2} \int \frac{d^2 k_{\perp}'}{k_{\perp}'^2} \int d^2 k_{\perp} \left(\frac{k_{\perp} \times k_{\perp}'}{M^2} \right)^2 \frac{\text{Tr}\{\gamma_{-} \hat{\gamma}^* \gamma_{+} \hat{\gamma}\}}{\hat{k} \hat{k}^*} \\
 & \sim \left(\int^{|k_{\perp}''| \ll M} \frac{d^2 k_{\perp}''}{k_{\perp}''^2} \right) \int \frac{d^2 k_{\perp}' d^2 k_{\perp}}{k_{\perp}'^2 k_{\perp}^2} \left(\frac{k_2 k_3' - k_3 k_2'}{M^2} \right)^2 \\
 & \sim \left(\int^{|k_{\perp}''| \ll M} \frac{d^2 k_{\perp}''}{k_{\perp}''^2} \right) \int_{O(MS^{1/2})} \frac{d(k_{\perp}'^2)}{M^2} \int_{O(MS^{1/2})} \frac{d(k_{\perp}^2)}{M^2} \\
 & \sim S/M^2. \tag{6.8}
 \end{aligned}$$

We can similarly add a soft gluon to each of the one gluon diagrams discussed in the last section and generate a high-energy amplitude of the same form. There is, however, clearly a divergence at $|k_{\perp}''|^2 = 0$ that we must discuss. First, however, we discuss the relevant color factors.

E. Two gluon color factors

There are two possible color factors for the transverse momentum diagram of Fig. 24. They are shown in Figs. 23(b) and 23(c) and have the form

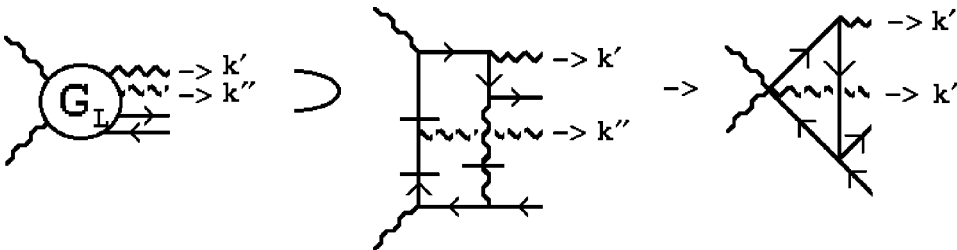


FIG. 26. A two gluon effective triangle diagram.

$$\text{(b) } \sum_{i,j} \text{Tr}\{\lambda_j \lambda_i \lambda_j \lambda_i\}, \quad \text{(c) } \sum_{i,j} \text{Tr}\{\lambda_i \lambda_j \lambda_i \lambda_j\}. \tag{6.9}$$

We discuss these two factors in a manner that will generalize when further gluons are added. The essential formula we need is

$$\lambda_i \lambda_j = \frac{2}{3} \delta_{ij} + \sum_k (if_{ijk} + d_{ijk}) \lambda_k \tag{6.10}$$

which, since f_{ijk} is antisymmetric and d_{ijk} is symmetric, implies that

$$\lambda_j \lambda_i + \lambda_i \lambda_j = \frac{4}{3} \delta_{ij} + 2 \sum_k d_{ijk} \lambda_k \tag{6.11}$$

and

$$\lambda_j \lambda_i - \lambda_i \lambda_j = -2i \sum_k f_{ijk} \lambda_k. \tag{6.12}$$

Therefore, the sum of the two color factors (6.9) is given by

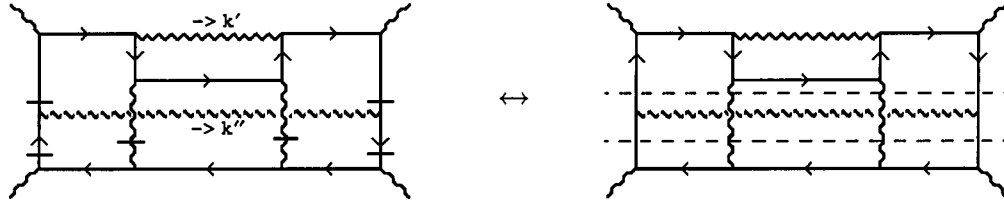


FIG. 27. A two gluon Feynman diagram with two cuts.

$$\begin{aligned}
 & \sum_{i,j} \text{Tr}\{\lambda_j \lambda_i \lambda_i \lambda_j + \lambda_i \lambda_j \lambda_i \lambda_j\} \\
 &= \sum_{i,j} \text{Tr}\left\{\left[\frac{4}{3} \delta_{ij} + 2 \sum_k d_{ijk} \lambda_k\right] \lambda_i \lambda_j\right\} \\
 &= \sum_{i,j} \text{Tr}\left\{\left[\frac{4}{3} \delta_{ij} + 2 \sum_k d_{ijk} \lambda_k\right] \left[\frac{2}{3} \delta_{ij} + \sum_l d_{ijl} \lambda_l\right]\right\} \\
 &= \sum_{i,j} \left[\frac{8}{9} \delta_{ij} + \frac{4}{3} \sum_k d_{ijk}^2\right] = 20 \frac{4}{9} \quad (6.13)
 \end{aligned}$$

and the difference of the two gives

$$\begin{aligned}
 \sum_{i,j} \text{Tr}\{\lambda_j \lambda_i \lambda_i \lambda_j - \lambda_i \lambda_j \lambda_i \lambda_j\} &= \sum_{i,j,k,l} \text{Tr}\{[-2if_{ijk} \lambda_k] \lambda_i \lambda_j\} \\
 &= \sum_{i,j,k} \text{Tr}\{[2if_{jik} \lambda_k][if_{ijl} \lambda_l]\} \\
 &= \sum_{i,j,k} \frac{4}{3} f_{ijk}^2 = 12. \quad (6.14)
 \end{aligned}$$

Both Eqs. (6.13) and (6.14) are expressed as a sum of squares of color factors where each individual term corresponds to a particular color for the gluon intermediate state. The states that contribute can be found by writing the left-side color factor as a sum over distinct intermediate states, as is effectively done in Eqs. (6.11) and (6.12). The full color factor can then be written, relying on the orthogonality of the intermediate states, as a sum of squares of the left-side factors. The quark-antiquark intermediate state can only carry zero or octet color. Correspondingly, since the total color of the intermediate state is zero, the gluon sums must also contribute either zero or octet color. This will continue to be the case when more gluons are present in the transverse momentum state. For the two gluon case, as illustrated in Fig. 28, in the symmetric color factor (6.13) the gluon sums give zero and octet color contributions, which both have even color

parity. In the antisymmetric factor (6.14) only the color octet with odd color parity contributes.

F. The color factor for the anomaly

Consider again the effective triangle diagram of Fig. 22. (As in the last section, we will initially discuss only the various anomaly contributions to G_L , with G_R kept fixed.) Comparing with the diagrams of Figs. 3 and 12(a), the twisted triangle diagram that should give an anomaly contribution to add to that of Fig. 26 is that shown in Fig. 29(a) and the corresponding full diagram is that of Fig. 29(b). As illustrated in Fig. 30 and in analogy with Fig. 13, Fig. 29(b) can be obtained by adding an exchanged gluon to the two cut amplitude of Fig. 30(a).

Again, in the anomaly region, with $|k'_\perp|^2 \ll |p'_\perp|^2, |p''_\perp|^2$, the exchanged gluon does not interfere significantly with the kinematics of taking the double discontinuity of Fig. 30(a). It is also clear from Fig. 30, that the on-shell lines of Fig. 29(b) correspond to physical double discontinuities of the G_L and G_R .

If we consider the order of λ matrix multiplication (following the quark arrow) we see that it is reversed for the two gluons in Fig. 29(a) compared to those in Fig. 26. As a result, if we add the two diagrams the anomaly is multiplied by the sum of the two color factors (6.13). As we have discussed, in this case there are separate contributions corresponding to whether the quark-antiquark pair is in a color octet or a color zero state.

G. Signature and color charge parity

To form signed amplitudes we consider, with the diagrams of Figs. 27 and 29(b), the corresponding diagrams for same helicity vector scattering. These are shown in Figs. 31(a) and 31(b), respectively. With flavor included, the left-hand couplings in these diagrams should be replaced by the full, flavor symmetric, couplings of Fig. 22(b), while the right-hand couplings should continue to be the analogue of

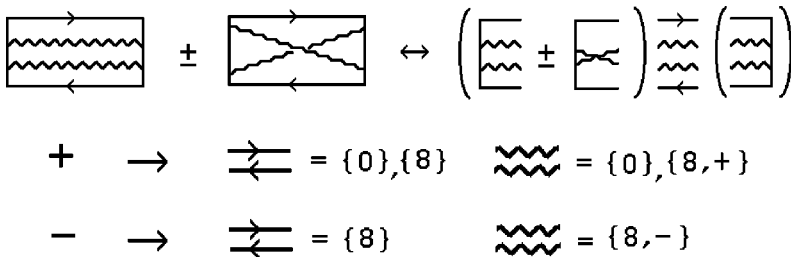


FIG. 28. Color breakdown of the intermediate state.

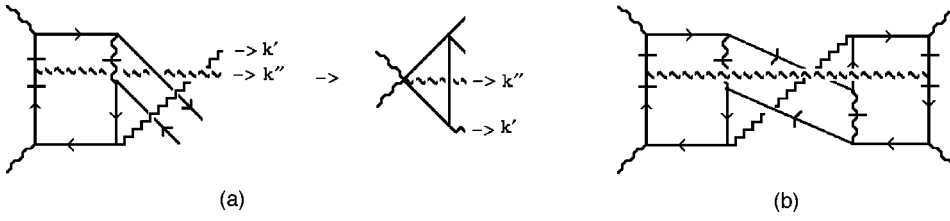


FIG. 29. (a) A twisted effective diagram. (b) The full twisted diagram.

Fig. 22(a). As in Fig. 18, we display the diagrams in two different ways, each of which will be simpler for particular arguments.

To discuss signature we focus on the first forms displayed. Comparing with our discussion of the diagrams of Fig. 20, we note that Figs. 31(a) and 31(b) again differ, kinematically, from Figs. 27 and 29(b), respectively, only in that $P_+ \rightarrow -P_+$ along the left-most vertical line. Therefore, if we evaluate the diagrams of Fig. 31 in the cross-channel physical region—with the sign of P_+ reversed—they will be kinematically identical, respectively, to Figs. 27 and 29(b) and will give identical anomaly contributions, but with $S \rightarrow -S$. Therefore, these diagrams have anomaly contributions with the opposite sign to those of Figs. 26 and 29(b) and in a vector theory would provide a cancellation. In the present case, since the color factors are the same, the anomaly contributions of the two diagrams of Fig. 31 add to those of Figs. 27 and 29(b) in the even signature amplitude and produce a cancellation in the odd signature amplitude.

As in our discussion of the one gluon diagrams, we can also obtain the signature from the CP symmetry properties of the intermediate transverse momentum state. We consider, first, properties of the gluon component. Since the gluons have only QCD vertices, they can have simple transformation properties under C and P separately. Applying color charge conjugation to Eq. (6.11) gives

$$\begin{aligned} [\lambda_j \lambda_i + \lambda_i \lambda_j] &\rightarrow (-1)^2 [\lambda_j^* \lambda_i^* + \lambda_i^* \lambda_j^*] = [\lambda_j \lambda_i + \lambda_i \lambda_j]^* \\ &= \frac{2}{3} \delta_{ij} + \sum_k d_{ijk} [\lambda_k]^*. \end{aligned} \quad (6.15)$$

The parity transformation reverses the transverse momentum of the gluons and so, because of the coupling (4.26) for the large transverse momentum gluon, again gives a minus sign. Therefore, the full effect of the CP transformation of the gluon component of the intermediate state is given by

$$\frac{2}{3} \delta_{ij} + \sum_k d_{ijk} [\lambda_k] \rightarrow -\frac{2}{3} \delta_{ij} - \sum_k d_{ijk} [\lambda_k]^*. \quad (6.16)$$

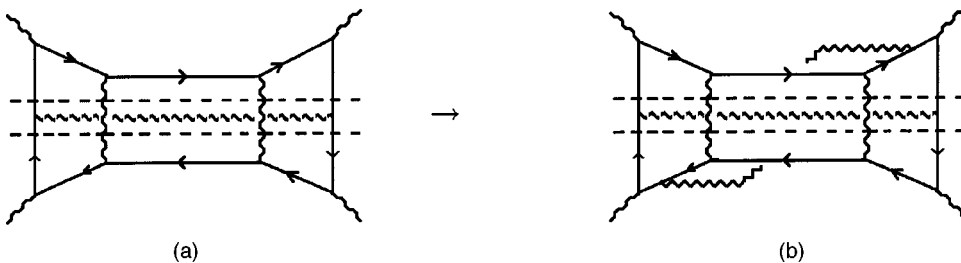


FIG. 30. Addition of an exchanged gluon to a two cut amplitude.

Comparing Eqs. (6.15) and (6.16) with Eq. (6.11) we observe that the color zero two gluon state carries negative CP and is separately even under C and odd under P . It therefore has “normal” color charge parity (equal to the number of gluons in the state) but has “anomalous” negative parity, producing an “anomalous” negative signature. The color parity of the octet gluon state is also well defined if we ignore $[\lambda_k] \rightarrow [\lambda_k]^*$ (which is, of course, compensated for by the quark-antiquark interchange discussed below) and is similarly even.

To discuss the CP transformation of the quark-antiquark pair we compare with our discussion in Sec. III E and note, first, that the left-side coupling of Fig. 31(b) can be obtained, diagrammatically, from that of Fig. 27 by quark-antiquark interchange. The left-side coupling of Fig. 31(a) can similarly be obtained from that of Fig. 29(b). In the even signature amplitude we must evaluate the diagrams of Fig. 31 with $P_+ \rightarrow -P_+$ compared to the other diagrams. Therefore, quark-antiquark interchange now gives three kinematic changes of sign

$$\begin{aligned} \text{(i)} \quad &k_\perp \rightarrow -k_\perp, \\ \text{(ii)} \quad &k'_\perp \rightarrow -k'_\perp \text{ from } P_+ \rightarrow -P_+, \\ \text{(iii)} \quad &k''_\perp \rightarrow -k''_\perp \text{ from } P_+ \rightarrow -P_+. \end{aligned} \quad (6.17)$$

When all four diagrams are added the amplitude is, kinematically, antisymmetric under quark-antiquark interchange. As a result, when the quark-antiquark pair has color zero it is, straightforwardly, negative under CP . Combined with the negative CP of the color zero two gluon state this gives no change under the full CP transformation, as is necessary to obtain an even signature amplitude.

When octet color is involved, the color effect of interchanging the quark-antiquark pair will, as we already noted above, again be $[\lambda_h] \rightarrow [\lambda_h]^*$. Therefore, with the negative sign coming from the kinematic interchange, the complete CP transformation on the quark-antiquark pair again combines with the octet part of Eq. (6.16) to produce an overall positive CP result for the full two gluon quark-antiquark state.

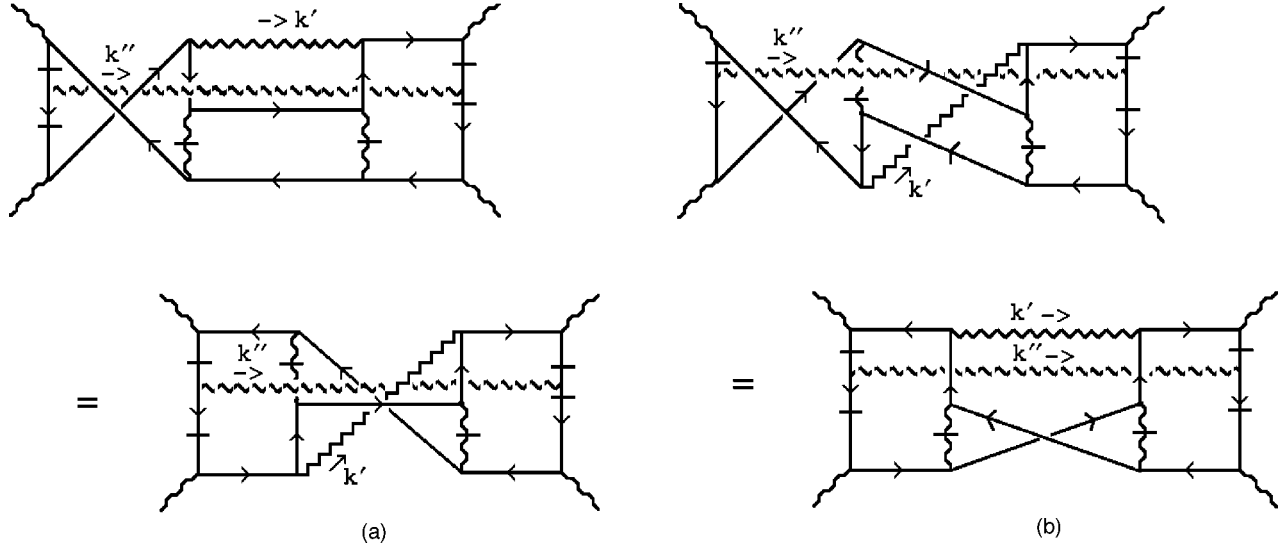


FIG. 31. Same helicity scattering diagrams with one soft gluon.

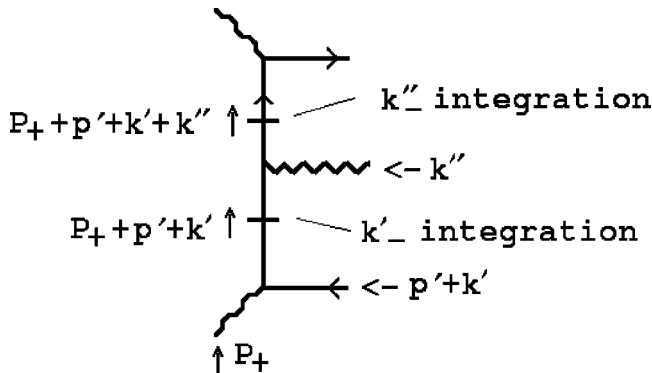
H. Infrared cancellations

Since Eq. (6.8) contains an infrared divergence (at $k_{\perp}''^2 \sim 0$), and there is no external color, there must be other anomaly contributions that cancel this divergence. Before discussing the possible diagrams that could be involved, it will be useful to first discuss the lower limit on the $k_{\perp}''^2$ integration in Fig. 27.

The momentum flow through the two lines that are put on-shell by the k'_{\perp} and k''_{\perp} integrations is shown in Fig. 32. Since k'_{\perp} is large and k'' is small, all the large momenta flow through both lines. Therefore, the large momenta are significantly constrained by the k' mass-shell condition before the k'' mass-shell condition is imposed. If we, temporarily, introduce a quark mass m then the k'_{\perp} mass-shell condition is $(P_{+} + p' + k')^2 = m^2$ and, with this constraint, the mass-shell condition for k''_{\perp} becomes

$$k''_{\perp} \sim \frac{-2k'_{\perp}(p' + k')_{\perp} + m^2}{P_{+}},$$

$$\underset{k''_{\perp} \rightarrow 0}{\sim} \frac{m^2}{S^{1/2}}. \quad (6.18)$$

FIG. 32. Momentum flow for the k'_{\perp} and k''_{\perp} integrations.

If k''_{+} is similarly constrained and (to justify the reduction to a transverse momentum diagram) we require $k_{\perp}''^2 \geq |k''_{-} k''_{+}|$, the lower limit for the k_{\perp}'' integration is

$$|k''_{\perp}|^2 \sim \frac{m^4}{S} \quad (6.19)$$

and so an infrared divergence appears at $|k''_{\perp}|^2 = 0$, as $S \rightarrow \infty$, of the form

$$\int_{|k''_{\perp}|^2 \sim m^4/S} \frac{d^2 k''_{\perp}}{k''_{\perp}{}^2} \sim \ln S - \ln m^4. \quad (6.20)$$

As we discuss briefly in the next section, we expect the cancellation of the infrared divergence (6.20) to be a consequence of a Ward identity that results from attaching the soft gluon at every possible point around the effective triangle diagram. Consider, therefore, the attachment of the soft gluon, in G_L , according to the other possibilities illustrated in Fig. 25. With the attachment shown in Fig. 25(b) we obtain the full diagrams shown in Fig. 33.

The mass-shell condition now has the form (6.7) and so, if the lower limit for the k'_{+} integration still has the form (6.18), requiring $|k'_{\perp}|^2 > k'_{+} k'_{-}$ gives the lower limit

$$|k'_{\perp}|^2 \sim \frac{m^2 M}{S^{1/2}}. \quad (6.21)$$

Therefore, if the diagrams of Fig. 33 give anomaly contributions they will have, as a factor, an infrared divergence of the form

$$\int_{|k'_{\perp}|^2 \sim m^2 M/S^{1/2}} \frac{d^2 k'_{\perp}}{k'_{\perp}{}^2} \sim \frac{1}{2} \ln S - \ln m^2 - \ln M. \quad (6.22)$$

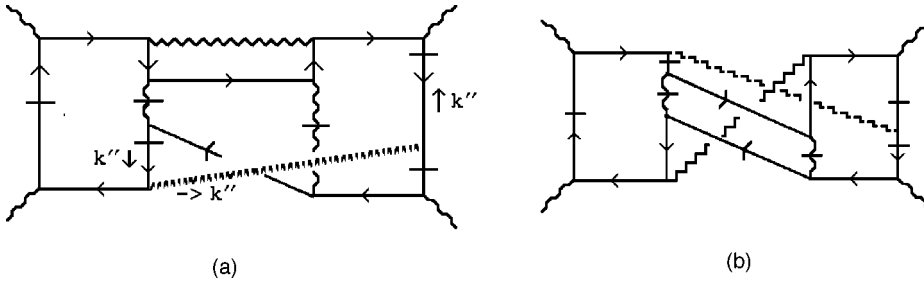


FIG. 33. Diagrams obtained with the soft gluon attachment of Fig. 25(b).

If, instead, one attachment of the soft gluon is that of Fig. 25(c) rather than that of Fig. 25(b), as we have just discussed, there will clearly be a similar infrared divergence.

There is, however, a major reason why the diagrams of Fig. 33, ultimately, do not give an anomaly contribution. Because of the location of the soft gluon attachment, the sign change (iii) in Eq. (6.17) will not be present when $P_+ \rightarrow -P_+$ in the diagrams appropriately related to those of Fig. 33 in the same sign helicity amplitude. As a result, in the even signature anomaly amplitude, the quark-antiquark intermediate state must be positive under CP . Alternatively, if we add all the diagrams related to those of Fig. 33 that give all possible contributions to each G_R , we will obtain G_R couplings to the quark-antiquark intermediate state that have negative CP . Therefore, when all diagrams related to those of Fig. 33 are added in the even signature amplitude, the resulting G_L requires positive CP for the quark-antiquark state, while the G_R requires negative CP . Consequently, if there is an anomaly contribution from any of the diagrams, it must cancel in the sum.

This last problem similarly applies to all diagrams in which one soft gluon attachment is as in Fig. 25(c) while the other attachment is that of Fig. 25(a). As we will shortly discuss there will, nevertheless, be important anomaly contributions from diagrams in which the attachments of the second gluon, in both G_L and G_R , are either of the form of Fig. 25(b) or Fig. 25(c). In this case, however, the second gluon necessarily has “finite” transverse momentum and so can not produce an infrared divergence.

To look further for a divergence that could cancel that due to Fig. 27, we must consider whether there are any new kinematic configurations, generating the anomaly and involving a soft gluon, that cannot be viewed as a soft gluon accompanying the one gluon enhancement diagrams. In fact, if we are considering the attachment of the soft gluon at every possible point around the effective triangle diagram, there is one possibility that we have not yet included or discussed. This is to interchange the momenta of the two gluons involved in Fig. 26. In Fig. 34 we show the full diagram obtained from Fig. 27 by interchanging k' and k'' in one side of the diagram relative to the other. The soft gluon is again indicated by a broken line. (Note that Fig. 34 is symmetric with respect to k' and k'' , if we interchange the roles of G_L and G_R .)

If we interchange k' and k'' in Fig. 26, then the large transverse momentum flows into the triangle diagram at the left-most vertex while the single gluon vertex carries only small transverse momentum. This does indeed give an anomaly contribution. This contribution has, however, some

different properties compared to those we have so far discussed. In Fig. 35 we compare the large momentum route for k' with the possible routes for k'' , around the same triangle.

We observe, first, that while the route for k' large was determined by the particles we wished to put on shell, there are two possible routes if k'' is large. As illustrated, it could flow through either one or two quark propagators. From Eqs. (4.21) and (4.22), we see that the anomaly contribution is obtained from an expansion in powers of $|k''_{\perp}/p'_{\perp}|$ (in which the first term does not contribute). Consequently, if k'' appears in only one propagator, rather than two, the anomaly contribution will be reduced by a factor of $\frac{1}{2}$ (in the even signature amplitude where both chiralities are added for each propagator). The sign will also be opposite. This is the normal ambiguity of the ultraviolet anomaly, that occurs because of the choice of momentum routing, which we expect to be determined by a Ward identity.

If k' is small, the k'' mass-shell condition does not constrain the large transverse momentum (p'_{\perp}) involved in the k'_{\perp} mass-shell condition. As a result, the k'_{\perp} mass-shell condition gives a constraint similar to Eq. (6.7), i.e.,

$$k'_{\perp} \sim \frac{p'^2}{P_+} \sim \frac{\epsilon M S^{1/2}}{S^{1/2}} \sim \epsilon M. \quad (6.23)$$

Since the k'_+ integration in G_R has the lower limit (6.18), we will again obtain an infrared divergence of the form of Eq. (6.22). In this case, however, since there is a gluon attached to both the left and right side quark lines, there is no CP conflict. Also, from Fig. 36, it is clear that neither gluon interferes with the kinematics of the quark subamplitude, which remains such that the vector meson lines can consistently be placed on shell. In fact, if the anomaly has the sign and magnitude obtained from the second routing of Fig. 35(b) (which is the “normal” routing), there will be a can-

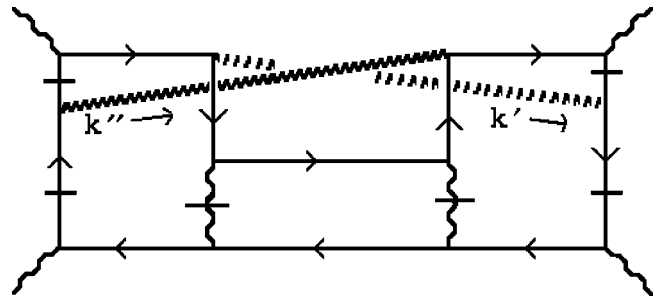


FIG. 34. The diagrams obtained by interchanging k' and k'' in Fig. 27.

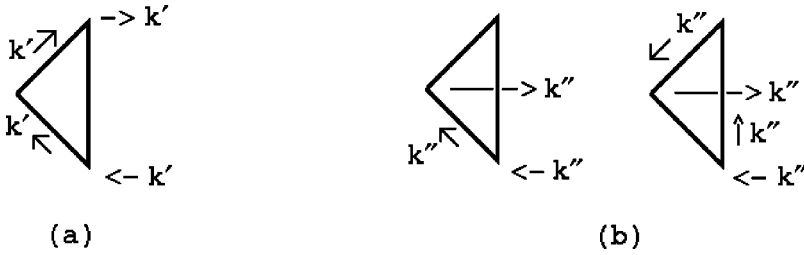


FIG. 35. (a) Momentum route for k'_{\perp} . (b) Possible routes for k''_{\perp} .

cellation with the divergence obtained from Fig. 27 when the diagram of Fig. 34 is added and the two contributions, from k'' large and k' small, and k' large and k'' small, are combined.

At this point we note that k' is the total momentum flowing in at a “vector” vertex of an effective triangle diagram with an anomaly. In this case, as we discuss in the next section (and illustrate for the usual triangle anomaly in Appendix C), we expect that the appropriate Ward identity, which would determine which routing in Fig. 35(b) is correct, will involve both the large internal momentum region of the triangle diagram that generates the anomaly and a small internal momentum region that produces a very different kinematic form, containing the “anomaly pole.” The discussion of the anomaly pole and pion wee gluon couplings that we have given in Ref. [8] should, essentially, carry over to an infra-red analysis of effective triangle vertices that would be the analogue of the ultraviolet analysis presented in this paper. This analysis must be carried out before we can establish, in detail, how the (Reggeon) Ward identities are satisfied, and that infrared divergences are indeed eliminated when the diagram of Fig. 34(a) is added to that of Fig. 27.

I. Anomalous color parity gluons

In the final form of two gluon anomaly contributions that we consider the second gluon transverse momentum k''_{\perp} is neither very small, nor grows with S . It is “finite,” i.e., $O(M^2)$. In the diagrams we consider, the above discussion implies that the kinematics of the anomaly prevent the second gluon from carrying very small transverse momentum. In particular, we consider diagrams of the form shown in Fig. 37, in which the second gluon attachment is the same in both G_L and G_R , and has the form of either Fig. 25(b) or Fig. 25(c). The broken gluon line in these diagrams now indicates finite transverse momentum and the lines put on shell correspond, as illustrated, to two cuts through each diagram. The combination of particle poles giving these two discontinuities, together with the off-shell loop, that occurs either at the top, in the middle, or at the bottom, in the three diagrams, is now responsible for the anomaly. [As usual, a closely related set of diagrams is obtained by simultaneously twisting both G_L and G_R in each of these diagrams. For Fig. 37(a) the same diagram is actually obtained, but the kinematic regions for the two gluons are interchanged.]

To form signed amplitudes, as before, we consider the same helicity scattering amplitudes shown in Fig. 38. Again we can argue that these diagrams are related to those of Fig. 37 by $P_+ \rightarrow -P_+$ and so the same anomaly amplitude is obtained, but with $S \rightarrow -S$. Therefore, these diagrams give

anomaly contributions that add to those of Fig. 37 in the even signature amplitude. However, as in our discussion of the diagrams of Fig. 23, because the finite gluon is not attached to the fast left side quark, the sign change (iii) in Eq. (6.17) will not be present when $P_+ \rightarrow -P_+$ in the diagrams of Fig. 38. Consequently, the G_L coupling obtained by adding the diagrams of Fig. 38 to those of Fig. 37, requires even CP for the quark-antiquark intermediate state. When the corresponding diagrams are added, this argument will similarly apply to G_R . As a result, the quark-antiquark state is necessarily positive under CP . This can be consistent with even signature for the complete intermediate state only if the two gluon state is also even under CP . This can, in turn, only be the case if the two gluon state carries antisymmetric octet color and so has “anomalous” odd color charge parity (not equal to the number of gluons).

In the two gluon anomaly contributions that we have discussed in previous subsections, the two gluon state has carried normal color charge parity because the addition of twisted diagrams gave the symmetric color factor. We must consider, therefore, whether there are also “twisted diagrams” related to those of Fig. 37 which cancel the antisymmetric part of the color factor.

Twisted diagrams related to the diagrams of Fig. 37 are shown in Fig. 39. For Figs. 39(a) and 39(b), the color factor is indeed reversed compared, relatively, to Figs. 37(a) and 37(b). Also, it is clear that, in Figs. 39(a) and 39(b), the appropriate (hatched) lines can be consistently placed on shell. [This is not true for other diagrams that could, potentially, be related, by twisting, to either of Fig. 37(a) or 37(b).] Therefore, as before, adding the diagrams of Figs. 39(a) and 39(b) to those of Figs. 37(a) and 37(b) gives the symmetric color factor and so, because the quark-antiquark state has even CP , the anomaly contribution must cancel in the sums of these diagrams.

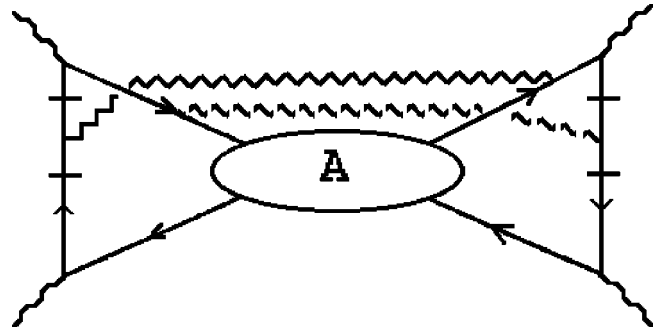


FIG. 36. Two gluons accompanying the quark subamplitude.

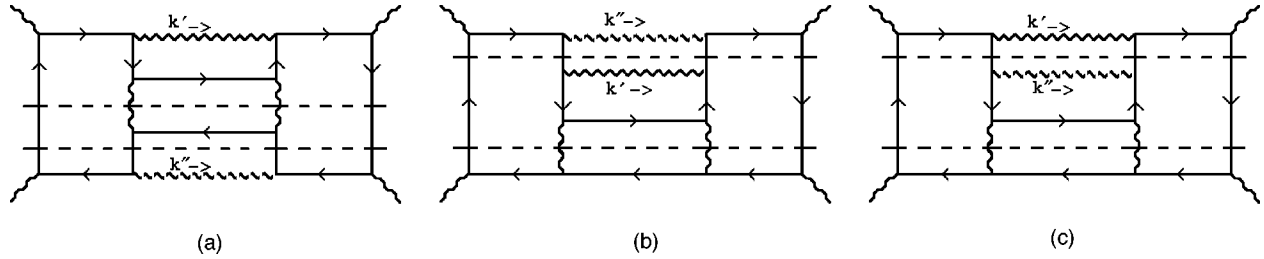


FIG. 37. Gluon attachments. (a) As in Fig. 25(b) or (b) and (c), as in Fig. 25(c).

Both Figs. 39(c1) and 39(c2) can be regarded as twisted relative to Fig. 37(c). For Fig. 39(c1) the color factor is reversed compared to Fig. 37(c), but the hatched lines clearly cannot be consistently placed on shell in the physical region. For Fig. 39(c2) it seems probable that the hatched lines can be placed on shell consistently, even though the necessary cuts would cross. The issue is irrelevant, however, since Fig. 39(c2) has the same color factor as Fig. 37(c). In fact, there is no twisted diagram corresponding to Fig. 37(c) which has a reversed color factor and in which all the necessary hatched lines can be consistently placed on shell.

Since we can regard the color factor for Fig. 37(c) as the sum of the symmetric and antisymmetric factors, the antisymmetric, odd color parity, component will be selected for the anomaly contribution from this diagram (and it's same helicity counterpart). Similarly for Fig. 39(c2), if it contributes. Together with the contribution of corresponding diagrams obtained by twisting both G_L and G_R , these will be the only anomaly contribution from diagrams in which the second gluon carries “finite” transverse momentum. In all cases, the second gluon is attached as in Fig. 25(c), and not as in Fig. 25(b). The finite gluon contributions have the important property that the two gluon state carries “anomalous color parity.” This is significant because, as we emphasized in the Introduction, Reggeized gluon exchanges that appear in vector theory perturbative calculations [1–7] carry normal color parity. The appearance of anomalous color parity gluon states is, therefore, a direct consequence of the presence of the anomaly.

J. General multigluon color factors

Before considering more complicated multigluon configurations we give a general discussion of multigluon color factors which generalizes the previously discussion of two gluon color factors. We note first that we can obtain Eqs. (6.11) and (6.12) from Eq. (6.10) by a more general argument than just the symmetry and antisymmetry of the d and f tensors. Consider a product of λ matrices

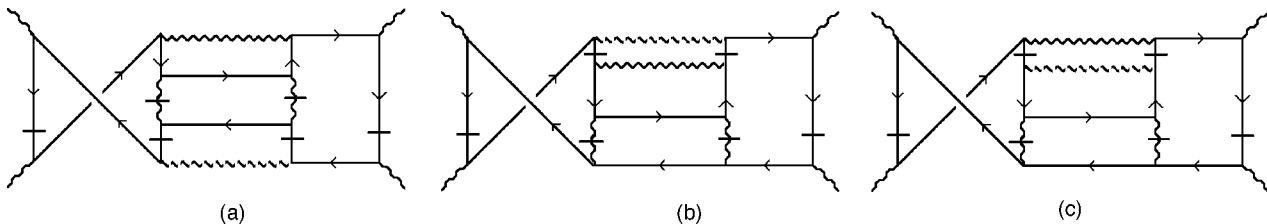


FIG. 38. Same helicity diagrams related to the diagrams of Fig. 37.

$$P_{1n} = \prod_{j=1}^n \lambda_{i_j} \tag{6.24}$$

together with the product taken in the reverse order

$$P_{n1} = \prod_{j=n}^1 \lambda_{i_j}. \tag{6.25}$$

Using Eq. (6.10) extensively we can write

$$P_{1n} = A_{1n} + \sum_k B_{1nk} \lambda_k, \tag{6.26}$$

where A_{1n} multiplies the unit matrix and both $A_{1n} = A_{i_1, i_2, \dots, i_n}$ and $B_{1n} = B_{i_1, i_2, \dots, i_n, k}$ contain combinations of f and d tensors. Similarly, we can write

$$P_{n1} = A_{n1} + \sum_k B_{n1k} \lambda_k. \tag{6.27}$$

Equations (6.26) and (6.27) decompose P_{1n} and P_{n1} , respectively, into a sum of color singlet and color octet contributions.

It follows from the hermiticity of the λ_i that

$$(P_{n1})^T = \prod_{j=n}^1 (\lambda_{i_j})^T = \prod_{j=n}^1 (\lambda_{i_j})^* = (P_{1n})^*, \tag{6.28}$$

where $(\dots)^T$ denotes transposition and $(\dots)^*$ denotes complex conjugation. Equivalently,

$$P_{n1} = [(P_{1n})^T]^*. \tag{6.29}$$

As a result

$$A_{n1} = A_{1n}^*, \quad B_{n1k} = B_{1nk}^* \tag{6.30}$$

or, equivalently,

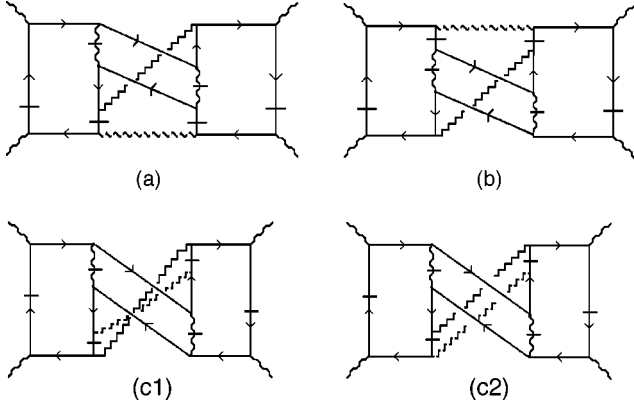


FIG. 39. Diagrams related to the diagrams of Fig. 33 by twisting.

$$\begin{aligned}
 P_{1n} + P_{n1} &= 2 \operatorname{Re}(A_{1n}) + 2 \operatorname{Re}(B_{1nk})\lambda_k \\
 P_{1n} - P_{n1} &= 2i \operatorname{Im}(A_{1n}) + 2i \operatorname{Im}(B_{1nk})\lambda_k
 \end{aligned}
 \quad (6.31)$$

which gives Eqs. (6.11) and (6.12), as a very simple case.

Since the f and d tensors are both real, it follows from Eq. (6.10) that a factor of i is always accompanied by an f tensor. Therefore, the real and imaginary parts of both A_{1n} and B_{1n} contain, respectively, even and odd numbers of f tensors. If we then consider

$$\operatorname{Tr}\{\sum_{i_1, i_2, \dots, i_n} (P_{1n} \pm P_{n1})(P_{1n})\} \quad (6.32)$$

the distinct color of A_{1n} and B_{1n} and the distinct symmetry properties of the real and imaginary coefficients implies that

$$\begin{aligned}
 &\operatorname{Tr}\{\sum_{i_1, i_2, \dots, i_n} (P_{1n} + P_{n1})(P_{1n})\} \\
 &= 2\sum_{i_1, i_2, \dots, i_n} \{[\operatorname{Re}(A_{1n})]^2 + [\operatorname{Re}(B_{1n})]^2\}
 \end{aligned}
 \quad (6.33)$$

which is a sum of the squares of color factors for color zero and color octet states which contain an even number of f tensors and so describe normal color parity gluon states. Similarly,

$$\begin{aligned}
 &\operatorname{Tr}\{\sum_{i_1, i_2, \dots, i_n} (P_{1n} - P_{n1})(P_{1n})\} \\
 &= -2\sum_{i_1, i_2, \dots, i_n} \{[\operatorname{Im}(A_{1n})]^2 + [\operatorname{Im}(B_{1n})]^2\}
 \end{aligned}
 \quad (6.34)$$

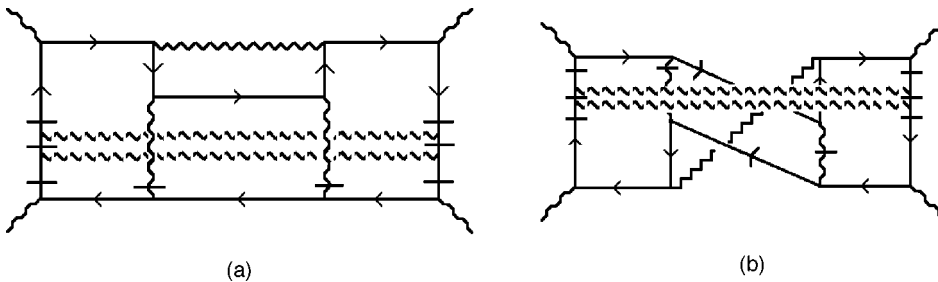


FIG. 41. Diagrams with two soft gluons.

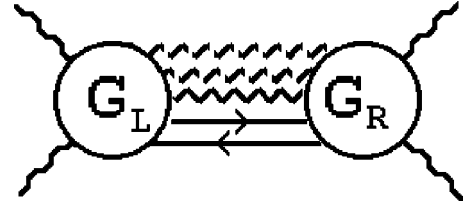


FIG. 40. A transverse momentum diagram with two soft gluons.

which is a similar sum of squares of color factors which, because they contain an odd number of f tensors, describe gluon states with anomalous color charge parity.

In the two gluon states that we have so far considered, all color factors apart from the first term in Eq. (6.34) have appeared. This term corresponds to a color zero anomalous color parity multigluon configuration. It will appear in the three gluon diagrams that we discuss next. We continue to confine our discussion to a single large transverse momentum gluon and consider only multiple soft or finite gluon contributions that do not involve any factors of $\ln S$. (In general, we anticipate that higher order logarithms lead to the separate Reggeization of each of the transverse momentum gluons in the diagrams we study.)

K. Two soft gluons

We begin with two soft gluons and consider diagrams that contribute to the transverse momentum diagram of Fig. 40. We will straightforwardly obtain an anomaly enhanced amplitude, as before, from diagrams in which two soft gluons are attached to the external effective point vertices, as illustrated in Fig. 41.

Because all the large momenta pass through both soft gluon attachments and are constrained by the k'_- integration, the infra-red scale is the same for both and is $m^2/S^{1/2}$, as in Eq. (6.18) and (6.19). Infrared cancellations can, presumably, be discussed in the same manner as in our discussion of one soft gluon diagrams. The twisted diagram of Fig. 41(b) again reverses the color matrix multiplication of Fig. 41(a) and so the sum of the two diagrams gives a color factor of the form of Eq. (6.33), corresponding to normal color parity for the complete three gluon transverse state.

To check that the anomaly amplitude obtained is even signature we note that the anomaly diagrams in the same sign helicity amplitude will again be related to the opposite sign diagrams by $P_+ \rightarrow -P_+$. For example, the diagram of Fig. 37(a) will be related to a same sign helicity amplitude diagram as illustrated in Fig. 42. Since the color factors are the same, these amplitudes are again related by $S \rightarrow -S$ and

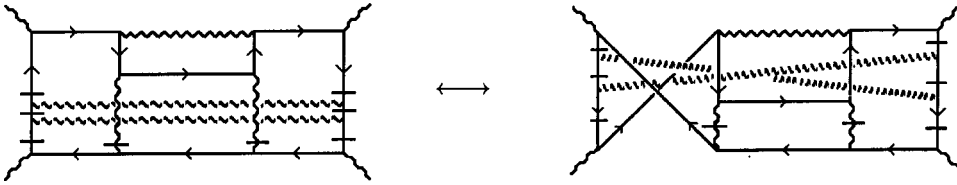


FIG. 42. Related diagrams in different helicity amplitudes.

will add in the even signature amplitude (and would cancel in a vector theory).

As before, the full gluon state will have negative parity because of the single large transverse momentum gluon. Combined with the negative (normal) color parity this implies that the three gluon state is even under CP . Repeating the discussion of the quark-antiquark state that we gave for the one soft gluon amplitudes we find that there is an additional change of sign from $P_+ \rightarrow -P_+$ that results from the additional soft gluon. As a result, quark-antiquark interchange gives no kinematic change of sign and the color charge parity transformation simply gives $\lambda_h \rightarrow \lambda_h^*$. Consequently, the full quark-antiquark-multigluon intermediate state is even under CP , as required for even signature. (We should note, however, that although the color zero three gluon state has normal color charge parity, it is “anomalous” in that it has negative parity, giving an “anomalous” positive signature.)

L. Color zero anomalous color parity

Consider, next, adding a soft gluon to the diagrams of Figs. 37(c) and 38(c), in which there is already one finite transverse momentum gluon present. If the soft gluon is attached to the left and right side quark lines, the resulting opposite sign and same sign helicity diagrams are shown, respectively, in Figs. 43(a) and 43(b).

The color factor for both diagrams is the same, i.e.,

$$\sum_{i,j,k} \text{Tr}\{\lambda_k \lambda_j \lambda_i \lambda_j \lambda_k\}. \tag{6.35}$$

If we pick out the color zero intermediate state then the color factors on the left and right side of the diagrams must separately factor into traces. Therefore, we can write

$$\begin{aligned} \sum_{i,j,k} \text{Tr}\{\lambda_k \lambda_j \lambda_i \lambda_j \lambda_k\} &\sim \sum_{i,j,k} \text{Tr}\{\lambda_j \lambda_i \lambda_k\} \text{Tr}\{\lambda_i \lambda_j \lambda_k\} + \dots \\ &\sim \sum_{i,j,k} f_{ijk}^2 + \dots, \end{aligned} \tag{6.36}$$

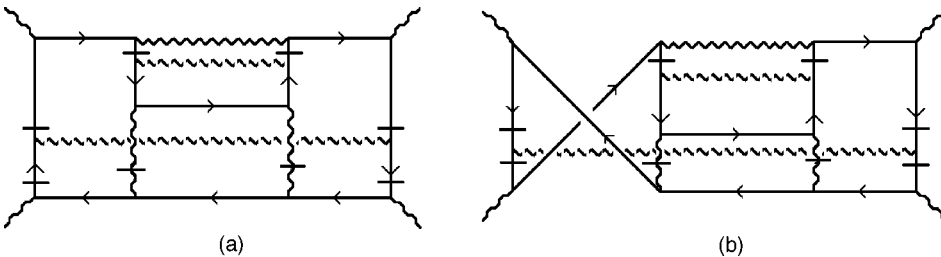


FIG. 43. Anomalous color parity diagrams with one soft and one finite gluon.

where the term we have shown explicitly is the color zero, anomalous (even) color parity, term.

Because the diagrams of Fig. 43 contain one less gluon attached to the fast quark lines than the diagrams of Fig. 42, the quark-antiquark component of the transverse state, in the even signature amplitude, will be odd under CP . Therefore, to obtain even signature overall the gluon component must also be odd under CP , implying that is even under color charge conjugation. Consequently, the anomalous color parity term, shown explicitly in Eq. (6.36), is selected for the color zero component of the combination of the diagrams of Fig. 43 in the even signature amplitude.

M. Multigluons

Clearly we could generalize the foregoing discussion to a variety of multigluon configurations involving combinations of soft and finite gluons, with effective vertices of the form illustrated in Fig. 44. However, having established the coupling of color zero anomalous color parity gluons, we have all the general properties that we require for the discussion of the next section.

Since a large transverse momentum gluon can give a scaling contribution of the form

$$\sim \int_{(k_{\perp}'')^2 \sim \sqrt{s} (k_{\perp}'')^2} d^2 k_{\perp}'' \tag{6.37}$$

it is also possible for additional large transverse momentum gluons to participate in the enhancement effect. Potentially, this could be an elaborate phenomenon involving, presumably, the reggeization of both quarks and gluons and, in higher orders, scaling properties of Reggeized gluon interactions, as well as the evolution of α_s . However, since we will argue, in the next section, that large transverse momentum anomaly contributions are unphysical, there seems little point in exploring the issue any further. In part, we discuss the analogous infrared phenomenon in the next section.

VII. REGGEON WARD IDENTITIES, CUTOFFS, AND INFRARED DIVERGENCES

Our calculations in the previous sections have demonstrated that the anomaly enhanced diagrams, some of which

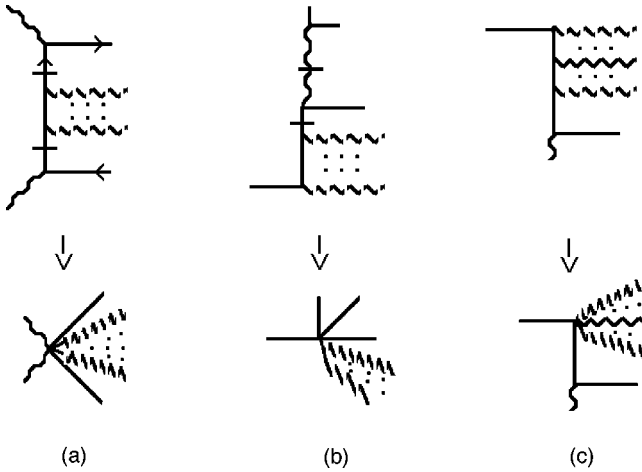


FIG. 44. Multi gluon effective vertices.

contain anomalous gluons, provide the dominant contribution in the exchange channel we have considered. However, as we remarked in the Introduction, we believe that the power enhancement involved should not be present in physical amplitudes. Assuming that there is no perturbative cancellation, via some mechanism that has yet to be elucidated, then obtaining “physical” amplitudes without the enhancement is, *a priori*, a challenging problem.

In this section we will briefly outline how we anticipate the desired physical amplitudes can be obtained. The essential point will be that the contribution of the anomaly diagrams is very different if we take the Regge limit before or after the removal of an ultraviolet transverse momentum cutoff. This cutoff introduces infrared divergences and if it is removed only at a very late stage, as we will propose, then the result obtained will also depend on whether all orders sums are performed before or after it is removed and on how, and at what stage, infra-red cut-offs (in the form of gluon and quark masses) are removed. This ambiguity is the essence of the anomaly and it would not be surprising if there is a unique procedure that is necessary to obtain the right “physical” answer.

As we have already noted, both in the Introduction and in the previous section, a study of the infrared anomaly contributions of the diagrams we have considered, that matches the present study of ultraviolet contributions, will be necessary before any detailed arguments can be carried through. To fully elucidate infrared anomaly contributions it will surely be necessary to abandon the restriction to forward kinematics and transverse polarizations that has greatly simplified the foregoing discussion. Nevertheless, based on our experience with hadron scattering amplitudes [8], we believe that a complete procedure for obtaining physical amplitudes can be developed utilizing the following, briefly summarized, properties. Our hope is that since the present starting point is much simpler than the hadronic problem, the analysis will be correspondingly more straightforward.

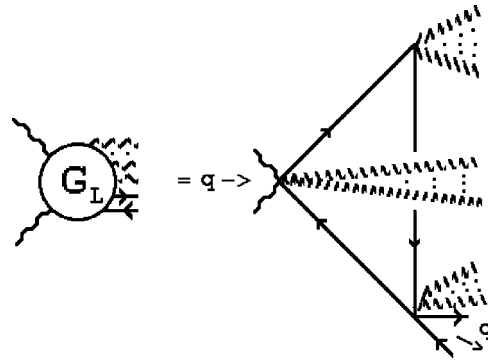


FIG. 45. An infrared red effective triangle diagram.

A. Ward identity consequences and a transverse momentum cutoff

Gauge invariance implies that a general amplitude $\langle A_\mu(q) \dots \rangle$ with all (external) lines on shell except for one gluon that carries four momentum q satisfies the simple Ward identity

$$q_\mu \langle A_\mu(q) \dots \rangle = 0. \tag{7.1}$$

This identity usually follows [12], at a given order in perturbation theory, only after the zero momentum gluon has been attached to the remainder of the diagram at all possible points. It is well known that this identity, in turn, implies that the gluon amplitude vanishes at zero four momentum. Also, from analogous Ward identities [12], a similar result holds when more than one gluon carriers vanishing four momentum. [If the gauge symmetry is spontaneously-broken then, of course, the Ward identities corresponding to Eq. (7.1), such as the “electroweak Ward identities” referred to in Sec. VC, have additional mass terms which prevent the infrared vanishing of amplitudes.]

The vanishing of a loop amplitude when external momenta are small compared to (“finite”) internal momenta also implies, generally, a suppression of internal momenta that are large compared to, finite, external momenta. If, however, there is an external axial current producing an anomaly contribution in a loop, then the situation is different. In this case, as we briefly review in Appendix C, in addition to the well-known anomalous Ward identity [13] for the axial current, vector Ward identities require a cancellation between separate contributions, with different kinematic structure, from large and small internal momentum regions. In particular, the large momentum anomaly contribution (C5) cancels with an infrared term that, in special momentum configurations (and only when the quarks are massless), reduces to a simple pole in the axial vector channel. This is the “anomaly pole” that can, in the right circumstances, be interpreted as a Goldstone boson pole, signaling chiral symmetry breaking. In addition to the discussion in Appendix C, a detailed analysis of the anomaly pole, and the internal momentum region generating it, can be found in Ref. [8].

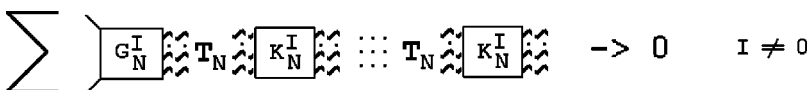


FIG. 46. Iteration of a gluon kernel K_N .

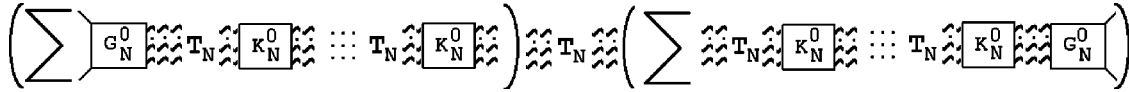


FIG. 47. Isolation of the divergence associated with T_N .

In general, the above properties of gluon amplitudes, as functions of four-dimensional momenta, transfer directly [14] to corresponding properties for the multigluon (multi-Reggeon) transverse momentum couplings that we discuss in this paper, as functions of transverse momenta. The linear vanishing when transverse momenta are scaled to zero is sufficient to eliminate infrared divergences in the transverse momentum diagrams that we consider. If there is an anomaly in a transverse momentum coupling then, as we already noted in our discussion of infrared cancellations in Sec. VIH, there will be large and small internal momentum cancellations in the associated transverse momentum (Reggeon) Ward identities that parallel the cancellations that take place in the four-dimensional Ward identities. We expect that infrared divergences will be avoided, in part, by cancellation of the ultraviolet anomaly contributions we have found with infrared “anomaly pole” contributions. In fact, the coefficient of the anomaly in a transverse momentum coupling (which we did not determine) should be fixed by this cancellation.

If we impose a transverse momentum cutoff in all internal loop integrals of the diagrams we consider, this cutoff will be present in all transverse momentum diagram integrals and also within the loop integrals giving the external couplings. A cutoff in the transverse momentum diagram integrals is gauge invariant. *A priori*, however, in the external couplings such a cutoff is not gauge invariant. Therefore, if we take the regge limit with a transverse momentum cutoff imposed, it will be a serious question whether gauge invariance is restored by removing the cutoff after the limit. For the present we note only that in Ref. [8] we argued that anomaly pole contributions to infrared divergent amplitudes are gauge invariant. In the infrared region, we anticipate that there will be effective triangle diagram contributions to G_L and G_R couplings in which small transverse momentum gluons couple at all three vertices, as illustrated in Fig. 45. Based on the analysis of the previous section, both normal and anomalous color parity multigluon states should couple. With a transverse momentum cutoff imposed we expect that, when the total gluon transverse momentum vanishes the corresponding Ward identity will fail and there will be a non-zero coupling involving (when the quarks are massless) the anomaly pole. As a consequence, in transverse momentum diagrams of the form of Fig. 40 (with all gluons soft) there will be a logarithmic infrared divergence of the form

$$\int^{\lambda_{\perp}} \frac{dQ^2}{Q^2}, \tag{7.2}$$

where Q is the sum of all gluon transverse momenta.

A priori, the anomaly pole can appear in both G_L and G_R . However, at $t=0$, where the pole should appear, a finite lightlike momentum can be exchanged which can be parallel to either P_+ or P_- . We suspect that this light-cone momentum determines whether the pole appears via G_L or G_R . Clearly, a detailed study, of the kinematics and polarizations and kinematic forms associated with the appearance of the anomaly pole will be needed to be sure that, in the full amplitude, there is a simple pole with the appropriate residue to be associated with a pion.

B. Transverse momentum infrared divergences

Since the divergence (7.2) is not removed by external couplings (with a transverse cutoff), we must consider the effect of (all orders) interactions amongst the gluons. In the lowest-order diagrams we expect the divergence to be present for both normal and anomalous color parity gluon states. There may also be additional divergent transverse momentum configurations. However, as we now describe, when we sum all infrared divergences to all orders we expect that Eq. (7.2) is the only divergence that survives, and then only for anomalous gluons.

We can summarize the general nature of gluon infrared transverse momentum divergences and the role of a transverse momentum cutoff, very briefly, as follows. An expanded version of this summary can be found in Ref. [8]. For reasons that will become apparent in the next subsection we specifically discuss the case of SU(2) color, although all the properties we describe remain the same for higher gauge groups.

The self-interactions of an N gluon transverse momentum state T_N are described by dimensionless “kernels” $K_N^I(\dots, k_i, \dots, k'_j, \dots)$, where I denotes SU(2) color. [Each iteration of a kernel produces an additional factor of $\ln S$, or $(J-1)^{-1}$ in the J plane, which we will not show explicitly.] When the t -channel color is nonzero the infrared divergences related to Reggeization do not cancel and

$$\int \prod_{i=1}^N \frac{d^2 k_i}{k_i^2} K_N^I(\dots, k_i, \dots, k'_j, \dots) \rightarrow \infty, \tag{7.3}$$

$Q^2, I \neq 0 \quad (Q = \sum_i k_i).$

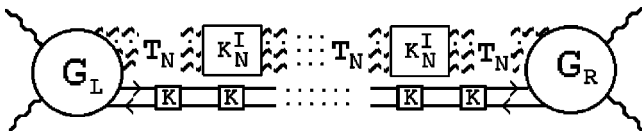


FIG. 48. A class of transverse momentum diagrams.

As a result, the sum of all diagrams in any colored channel exponentiates to zero as illustrated in Fig. 46. G_N^I is an external coupling analogous to the G_L and G_R appearing in the previous sections.

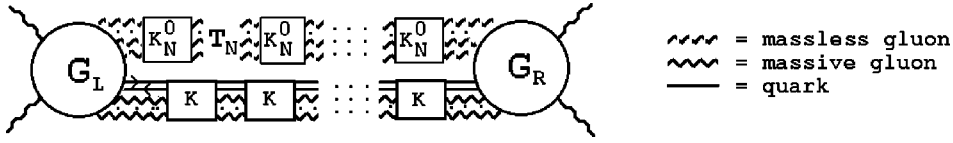


FIG. 49. General diagrams with a divergence.

When $I=0$ and $Q^2 \neq 0$, there is a cancellation of divergences in the K_N^0 . (This is the infrared finiteness property which is extensively exploited in BFKL applications.) At the leading-log level, infrared finiteness leads directly to conformal scale invariance. When renormalization effects are introduced, scale invariance is lost in the ultraviolet region. Scale invariance properties may still be present in the infrared region (in particular, they will be present if there is an infrared fixed point for the gauge coupling). In this case, the kernels K_N^0 will scale canonically as $Q^2 \rightarrow 0$ so that, with a transverse momentum cutoff λ_\perp ,

$$\int_{|k_i|^2, |k'_j|^2 < \lambda_\perp} \prod_i \frac{d^2 k_i}{k_i^2} \prod_j \frac{d^2 k'_j}{k_j'^2} K_N^0(k_1, \dots, k_N, k'_1, \dots, k'_N) \sim \int^{\lambda_\perp} \frac{dQ^2}{Q^2}. \quad (7.4)$$

The presence of the cutoff ensures that this divergence is unambiguously isolated from ultraviolet divergences with which it might mix.

This is the same divergence as Eq. (7.2), which appears in the lowest-order diagrams. The kernels K_N^0 have Ward identity zeroes which result in the special property that iteration of any K_N^0 does not increase the degree of divergence. Instead, there is a distinct contribution from each T_N and the residue of the divergence can be written in a factorized form, as illustrated in Fig. 47. If there is no Ward identity zero in the external couplings G_N^0 , Eq. (7.4) is a potential source of a simple infrared divergence at $Q^2=0$.

Similar properties to the above hold for the interactions of gluons with quarks. Crucially, however, there is no kernel describing a transverse momentum interaction between a quark-antiquark pair and an anomalous gluon state. This is because anomalous gluons couple only through an anomaly and anomalies can not occur within the two-dimensional kinematics that the kernels describe.

C. SU(2) color and Reggeon field theory

If we consider all the diagrams discussed in previous sections, generalized to include arbitrary numbers of gluons, and add both interactions amongst the gluons and between the quark-antiquark pair, we arrive at the set of transverse momentum diagrams shown in Fig. 48.

If the gluons are anomalous and carry zero color, they will have no interaction with the quark-antiquark pair and the divergence (7.4) will occur when the transverse momentum of all gluons is scaled to zero. As we discussed above, the anomaly pole should appear in the coefficient of this divergence, presumably, with the right kinematic structure to be interpreted as a pion pole. All other similar diagrams, in which either the color is nonzero or the gluons are not

anomalous will be exponentiated to zero by interactions that iterate the divergence. However, since the cutoff has still to be removed and it is unclear how to handle the infrared divergence, the result is still far from a sensible amplitude.

To obtain a more sensible result, we have to use a more sophisticated treatment of the infrared divergences. In particular, we initially take the SU(3) gauge symmetry of QCD to be partially broken to SU(2). We could motivate this by noting, first, that the structure of the anomaly diagrams is much simpler. Only odd numbers of anomalous gluons can carry color zero (because of the absence of the d tensor). An overall logarithmic infrared divergence will still occur, as we have discussed in the previous subsection, because of the unbroken SU(2) gauge symmetry. However, some gluons [that are massive and outside the SU(2) subgroup] will interact with the quark-antiquark pair. Also, we might hope to eliminate the divergence by averaging over the direction of the SU(2) subgroup within SU(3), as the transverse momentum cutoff is removed.

With these last observations in mind, it is easy to appreciate why Reggeon field theory (RFT) should be applied to the problem. In formulating the study of the QCD pomeron using RFT we have argued [7,10,14], that we should start from the Reggeon diagrams (or, equivalently, transverse momentum diagrams) in which the gauge symmetry is completely broken. With a transverse momentum cutoff, the gauge symmetry can first be restored to SU(2) and the resulting Reggeon diagrams can be described by supercritical Pomeron RFT—provided all infrared divergences can be absorbed into a “Pomeron condensate.”

For our present problem we anticipate applying RFT as follows. With SU(3) color broken to SU(2), we consider all diagrams of the form illustrated in Fig. 49. In these diagrams, anomalous gluons [within an SU(2) subgroup] accompany a quark-antiquark pair that is interacting with massive, Reggeized, gluons. The massive gluons are outside the SU(2) subgroup and carry nonzero transverse momentum. This set should map completely on to supercritical RFT diagrams containing both Pomerons [with the Pomeron being a massive Reggeized gluon plus anomalous SU(2) gluons] and a Reggeized Goldstone boson pion. In this mapping, the physical significance of the logarithmic infrared divergence would be clear. It would be identified as responsible for the appearance of a Pomeron condensate.

The restoration of SU(3) gauge symmetry would be described by the critical Pomeron [15] interacting with a Regge pole pion and (with the appropriate quark sector present [7,8]) the transverse momentum cutoff can be removed as part of the critical phenomenon. Also, as part of the critical phenomenon, the SU(2) direction of the pomeron condensate would be randomized within SU(3) and disappear. In effect, the infrared divergence, producing the condensate, would be

eliminated by averaging over the direction of the SU(2) subgroup within SU(3).

For hadron scattering it was important [8] that the Pomeron condensate could be related to an anomalous gluon component of the scattering states. This was necessary, first, because the γ_5 anomaly coupling of the pion to the Pomeron is produced by a product of three orthogonal γ matrices. To obtain this product, it was essential to have anomalous gluon components in both the scattering pion and the exchanged Pomeron. As we have seen, in electroweak scattering this requirement is absent because the vector mesons have elementary γ_5 couplings, which allow the anomalous gluons to appear in just the exchanged channel. However, the gluon components of the scattering states also seemed to be important for the higher-order Pomeron interactions needed to obtain the critical Pomeron. It may be, therefore, that RFT can only be consistently applied to the analysis of infrared divergences if the scattering vector mesons are also “hadronic.” That is, if they also have an anomalous gluon component, as they would have if they acquire their mass by absorbing Goldstone bosons resulting from QCD chiral symmetry breaking—with the quarks being color sextet quarks. The presence of the sextet quarks would produce [7,8] an infrared fixed point (in the massless quark theory) that would guarantee the infrared scaling of gluon kernels producing Eq. (7.4) and would also produce the “quark saturation” of QCD that we have argued is needed to obtain the critical Pomeron with no transverse momentum cutoff. Perhaps, all these features are needed to obtain a self-consistent description of the Regge limit for left-handed, massive, electroweak vector bosons.

VIII. CONCLUSIONS

We have demonstrated that the triangle anomaly appears in the couplings of transverse momentum diagrams that describe the high-energy scattering of $W^{\pm,0}$ vector mesons. When the full amplitudes are directly evaluated, without any special cutoff procedure, the anomaly produces an enhancement, by a power of the energy, that threatens the unitarity of the theory.

The most well-known consequence of a large momentum triangle anomaly is the famous anomalous Ward identity for axial currents [13]. Less emphasized is the feature that, in the presence of the anomaly, vector Ward identities are satisfied by a subtle cancellation between the contributions of large and small internal momentum regions. In the vector meson scattering we have discussed, an effective current component with an anomaly appears and it is the less emphasized feature that plays a crucial role. Even though there are no anomaly related cancellations between large and small internal momenta in the finite momentum Ward identities, in a left-handed gauge theory, it appears that the Regge limit enhances large transverse momentum regions such that there are cancellations of this kind in the transverse momentum (Reggeon) Ward identities. There is then an “anomaly problem” in the sense that the Regge limit result is very sensitive to the manipulation of ultraviolet and infrared cutoffs, as we have described.

In Appendix D, we raise the possibility that the occurrence of the anomaly enhancement phenomenon in the diagrams that we have discussed is related, via Ward identity contributions, to a more widespread phenomenon of large transverse momentum enhancement. If this is the case, then it is likely that the general transverse momentum diagram formalism will fail. Since there would then be no Reggeon diagram formalism, t -channel unitarity is also likely to fail. The conclusion, which is really the main conclusion of this paper, is that to use the transverse momentum diagram formalism (and therefore to ensure t -channel unitarity) it is essential to initially employ a transverse momentum cutoff.

In previous papers we have found that for bound-state amplitudes in QCD, the occurrence of anomalies in multi-Reggeon vertices (involving anomalous gluons) leads to an analogous sensitivity to infrared and ultraviolet transverse momentum cutoffs. We have argued that an ultraviolet cutoff should be kept until after physical scattering amplitudes have been derived via an analysis of infrared divergences. We anticipated that, without an initial cutoff, the ultraviolet anomaly effects would produce nonunitary power enhancement of the energy behavior of bound-state amplitudes. However, as we noted in the Introduction, accessing the anomalies in hadron amplitudes is very complicated and, therefore, it is much more difficult to appreciate their significance. In the electroweak amplitudes we have studied in this paper the anomaly appears immediately, because of the presence of elementary left-handed couplings. As a result the choice between bad, large transverse momentum based, high-energy behavior and infrared anomaly domination producing “nonperturbative” dynamics, is also immediately clear.

Potential nonunitary properties of electroweak high-energy scattering amplitudes may not be of great concern if, as is currently believed by many physicists, the gravitational interaction intervenes long before the relevant energies are reached. From this perspective, our study of electroweak amplitudes can be viewed as simply a technical exercise in which left-handed vector mesons are used to study how, with the cutoff manipulation we have described, the formation of QCD bound states, including confinement and chiral symmetry breaking, can take place via Regge limit infrared anomaly effects. Nevertheless, it seems hard to avoid the conclusion that if confinement and chiral symmetry breaking do not take place in this manner, then (assuming that it does not cancel) the power enhancement of quark-antiquark exchange by the ultraviolet anomaly will dominate any electroweak symmetry breaking mechanism that is perturbatively based.

Our point of view is that the unitarity of the electroweak part of the standard model is a deep constraint. Indeed, it could be that obtaining consistent high-energy scattering amplitudes for massive vector mesons, with left-handed couplings to quarks, may actually require QCD confinement and chiral symmetry breaking to take place via the anomaly, and may even, perhaps, require that the chiral symmetry breaking (of higher color quarks) is responsible for electroweak symmetry breaking.

We were led to the present investigation as an outcome of our study of the QCD Pomeron. For a long period of time we

$$\begin{array}{c}
\hat{\psi}(1-\gamma_5) \rightarrow \hat{\psi}^* \\
\uparrow \gamma_- \\
\hat{\psi}^*(1-\gamma_5) \leftarrow \hat{\psi}
\end{array}
\rightarrow
\begin{array}{c}
\hat{\psi} \hat{\psi}^* (1-\gamma_5) \gamma_- \hat{\psi}(1-\gamma_5) \hat{\psi}^* \\
= 2 \hat{\psi} \hat{\psi}^* \gamma_- \hat{\psi}(1-\gamma_5) \hat{\psi}^* = 4 \gamma_- \hat{\psi} \hat{\psi}^*
\end{array}$$

$$\begin{array}{c}
\hat{\psi}(1-\gamma_5) \rightarrow \hat{\psi} \\
\uparrow \gamma_- \\
\hat{\psi}^*(1-\gamma_5) \leftarrow \hat{\psi}^*
\end{array}
=
\begin{array}{c}
\hat{\psi}(1-\gamma_5) \rightarrow \hat{\psi} \\
\uparrow \gamma_- \\
\hat{\psi}^*(1-\gamma_5) \leftarrow \hat{\psi}
\end{array}
=
\begin{array}{c}
\hat{\psi}(1-\gamma_5) \rightarrow \hat{\psi} \\
\uparrow \gamma_- \\
\hat{\psi}^*(1-\gamma_5) \leftarrow \hat{\psi}^*
\end{array}
= 0$$

FIG. 50. Couplings to quark-antiquark transverse momentum states.

understood the crucial role of the anomaly in producing unitary high-energy amplitudes within QCD, but were unable to find a simple starting point from which to begin construction of such amplitudes. Then, in our most recent paper [8], we showed that wee gluon properties of the pion, obtained from the anomaly, provide such a starting point, at least in part. At the same time we realized that such properties should appear if the pion is extracted from the wee parton structure of an electroweak vector meson. This led us to the, a priori much simpler, problem of how an exchanged pion appears within the scattering of vector mesons. We now believe that the results of this paper will lead to an understanding of the pion which will, eventually, provide a simple starting point for the construction of QCD high-energy amplitudes.

ACKNOWLEDGMENTS

I am grateful to Jochem Bartels for useful criticism of a preliminary version of this paper. I am also grateful to Bill Bardeen for valuable discussion of electroweak Ward identity cancellations. This work was supported by the U.S. Department of Energy under Contract W-31-109-ENG-38.

APPENDIX A: COMPLEX NOTATION FOR TRANSVERSE γ MATRICES

To discuss high-energy vector meson scattering amplitudes involving (massless) fermion exchange, it is convenient to use a complex number notation [16] for both transverse momenta and γ matrices. In this formalism, the consequences of chirality conservation and a left-handed

gauge interaction are particularly apparent.

In addition to using conventional light-cone momenta $k_{\pm} = (k_0 \pm k_1)/\sqrt{2}$, we write

$$\hat{k} = k_2 + ik_3, \quad \hat{k}^* = k_2 - ik_3 \quad (\text{A1})$$

to describe transverse momenta. We then have

$$k_{\perp}^2 = \hat{k} \hat{k}^* \quad (\text{A2})$$

and

$$2k_{\perp} \cdot q_{\perp} = \hat{k} \hat{q}^* + \hat{k}^* \hat{q}. \quad (\text{A3})$$

We can also write

$$\begin{aligned}
\hat{k} \hat{q}^* &= (\hat{k}^* \hat{q})^* = k_2 q_2 + k_2 q_3 + i(k_2 q_3 - k_3 q_2) \\
&= k_{\perp} \cdot q_{\perp} + ik_{\perp} \times q_{\perp},
\end{aligned} \quad (\text{A4})$$

where

$$k_{\perp} \times q_{\perp} = |k_{\perp}| |q_{\perp}| \sin \theta \quad (\text{A5})$$

with θ the angle between the two vectors.

To describe transverse γ matrices, we similarly write

$$\hat{\gamma} = (\gamma_2 + i\gamma_3)/\sqrt{2}, \quad \hat{\gamma}^* = (\gamma_2 - i\gamma_3)/\sqrt{2}. \quad (\text{A6})$$

We then have

$$(\hat{\gamma})^2 = (\hat{\gamma}^*)^2 = 0, \quad \hat{\gamma} \hat{\gamma}^* + \hat{\gamma}^* \hat{\gamma} = 2 \quad (\text{A7})$$

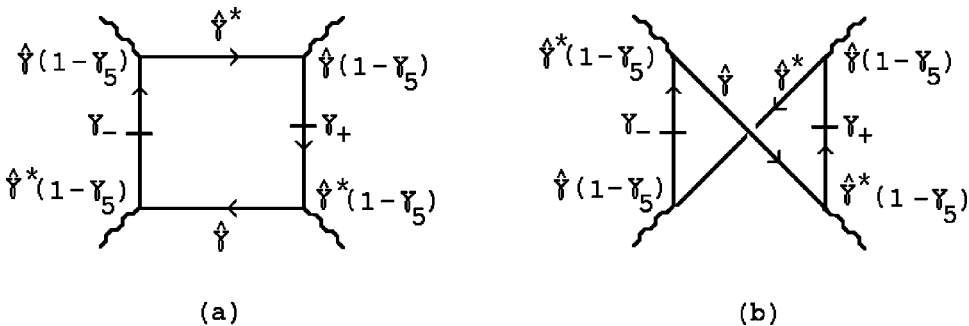
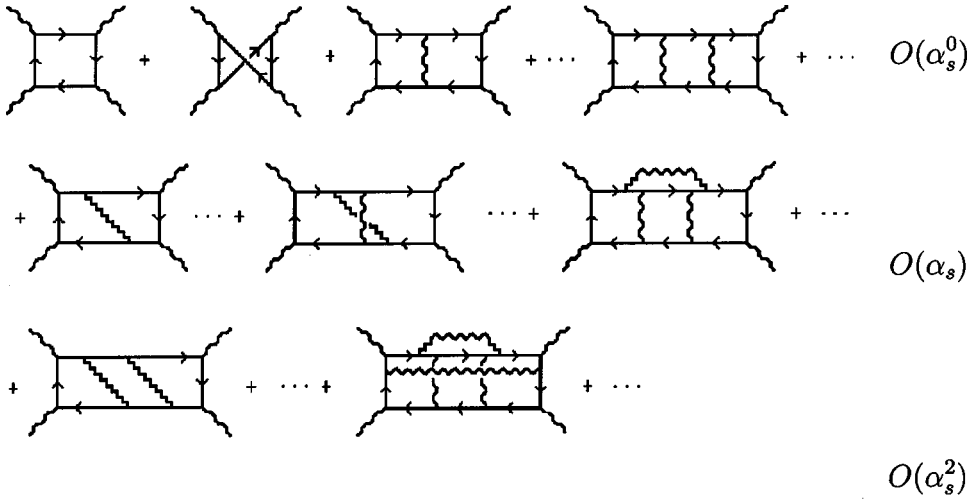


FIG. 51. Lowest-order diagrams.


 FIG. 52. Quark-antiquark exchange diagrams organized according to powers of α_s .

and we can write

$$2k_{\perp} = \hat{k} \hat{\gamma}^* + \hat{k}^* \hat{\gamma}. \quad (\text{A8})$$

In the Regge limit the transverse part of an exchanged fermion propagator dominates, i.e., for a massless fermion

$$\frac{\not{k}}{k^2} \rightarrow -\frac{1}{2} \left(\frac{\hat{\gamma}^*}{\hat{k}^*} + \frac{\hat{\gamma}}{\hat{k}} \right), \quad (\text{A9})$$

where the two terms represent the two different chiralities. For example, the transverse momentum integration of a quark-antiquark state with transverse momentum q_{\perp} and equal chiralities (opposite sign helicities) takes the form

$$\int d^2\hat{k}_1 d^2\hat{k}_2 \delta^2(\hat{q} - \hat{k}_1 - \hat{k}_2) \left(\frac{\hat{\gamma}}{\hat{k}_1} \otimes \frac{\hat{\gamma}^*}{\hat{k}_2} + \frac{\hat{\gamma}^*}{\hat{k}_1} \otimes \frac{\hat{\gamma}}{\hat{k}_2} \right), \quad (\text{A10})$$

where the \otimes sign indicates that the two γ matrices are separately associated with the two fermion lines. The contribution of a two fermion state with opposite chiralities is clearly analogous. However, the distinct combinations of same sign and opposite sign chiralities are exchanged and interact separately [16,11]. As we elaborate on briefly in Appendix B, the very different properties of the interaction of same sign and opposite sign chirality exchanges is of fundamental importance.

As we elaborate on briefly in Appendix B, the very different properties of the interaction of same sign and opposite sign chirality exchanges is of fundamental importance.

If we also define

$$\hat{\Pi}_+ = -\frac{1}{2} \hat{\gamma} \hat{\gamma}^*, \quad \hat{\Pi}_- = -\frac{1}{2} \hat{\gamma}^* \hat{\gamma}, \quad \Pi_+ = \frac{1}{2} \hat{\gamma}_- \gamma_+,$$

$$\Pi_- = \frac{1}{2} \gamma_+ \hat{\gamma}_- \quad (\text{A11})$$

then we can write

$$\gamma_5 = (\Pi_+ - \Pi_-)(\hat{\Pi}_+ - \hat{\Pi}_-). \quad (\text{A12})$$

Spinors in the subspaces $\Pi_- \hat{\Pi}_+$ and $\Pi_- \hat{\Pi}_-$ (or $\Pi_+ \hat{\Pi}_+$ and $\Pi_+ \hat{\Pi}_-$) carry opposite chirality, as is evident from the following relations:

$$\begin{aligned} \gamma_- \hat{\gamma} [1 - \gamma_5] \hat{\gamma}^* &= \gamma_- [1 + \gamma_5] \hat{\gamma} \hat{\gamma}^* = \gamma_- [1 - \Pi_- \hat{\Pi}_+] \hat{\gamma} \hat{\gamma}^* \\ &= \gamma_- \left(1 + \frac{1}{2} \hat{\gamma} \hat{\gamma}^* \right) \hat{\gamma} \hat{\gamma}^* = 2 \gamma_- \hat{\gamma} \hat{\gamma}^*, \end{aligned}$$

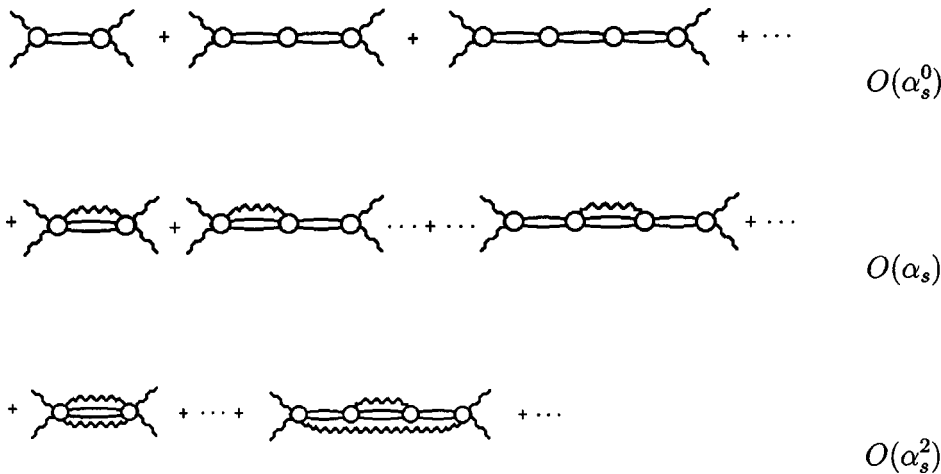


FIG. 53. Transverse momentum diagrams originating from the diagrams of Fig. 53.

$$\begin{aligned} \gamma_- \hat{\gamma}^* [1 - \gamma_5] \hat{\gamma} &= \gamma_- [1 + \gamma_5] \hat{\gamma}^* \hat{\gamma} = \gamma_- [1 + \Pi_- \hat{\Pi}_-] \hat{\gamma}^* \hat{\gamma} \\ &= \gamma_- \left(1 - \frac{1}{2} \hat{\gamma}^* \hat{\gamma} \right) \hat{\gamma}^* \hat{\gamma} = 0. \end{aligned} \quad (\text{A13})$$

Similarly, we can show that

$$\gamma_+ \hat{\gamma}^* (1 - \gamma_5) \hat{\gamma} = 0, \quad \gamma_+ \hat{\gamma} (1 - \gamma_5) \hat{\gamma}^* = 2 \gamma_+ \hat{\gamma} \hat{\gamma}^*, \quad (\text{A14})$$

$$\gamma_- \hat{\gamma} (1 + \gamma_5) \hat{\gamma}^* = 0, \quad \gamma_- \hat{\gamma}^* (1 + \gamma_5) \hat{\gamma} = 2 \gamma_- \hat{\gamma}^* \hat{\gamma}, \quad (\text{A15})$$

$$\gamma_+ \hat{\gamma}^* (1 + \gamma_5) \hat{\gamma} = 0, \quad \gamma_+ \hat{\gamma} (1 + \gamma_5) \hat{\gamma}^* = 2 \gamma_+ \hat{\gamma} \hat{\gamma}^*. \quad (\text{A16})$$

For a vector particle, with momentum along the 1 axis, the polarization vectors for states with helicity $\lambda = \pm 1$ are

$$\begin{aligned} \epsilon^\mu(\lambda = +1) &= -\frac{1}{\sqrt{2}}(0, 0, 1, i), \\ \epsilon^\mu(\lambda = -1) &= \frac{1}{\sqrt{2}}(0, 0, 1, -i). \end{aligned} \quad (\text{A17})$$

A vector boson with helicity $\lambda = -1$ can make a transition to a left-handed intermediate state quark via the emission of an antiquark. To calculate the scattering of a vector boson with helicity $\lambda = -1$ we introduce an initial coupling of $\bar{\psi} \hat{\gamma}^* (1 - \gamma_5) \psi$ and a final state coupling of $\bar{\psi} \hat{\gamma} (1 - \gamma_5) \psi$. Utilizing the above relations we find that, as illustrated in Fig. 50, there is only one nonzero coupling to potential quark-antiquark transverse momentum states that could be exchanged. As a consequence, if we consider the scattering of opposite helicity states there is only one possible lowest-order diagram, which is that shown in Fig. 51(a). The initial $\hat{\gamma}^* (1 - \gamma_5)$ vertex on the right-hand side of Fig. 50(a) represents the coupling of a vector boson with the same polarization, but opposite helicity (since it has opposite momentum along the one axis) to that of the left-hand side vector boson.

A simple way to see that the diagram of Fig. 1(a) contributes to opposite helicity scattering is to note that, because of the direction of the quark arrow, the intermediate state consists of a left-handed quark, which must be produced by a negative helicity vector boson, and a right-handed antiquark, which must be produced by a positive helicity vector boson. The direction of the arrow is fixed by choosing the left-hand vector meson to be the one with negative helicity. The diagram of Fig. 1(a) contributes to the A_{-+} helicity amplitude

$$\begin{aligned} &\sim \bar{\Upsilon}_+ \hat{\gamma}^* \frac{\hat{\Upsilon}_-}{\hat{p}'' - \hat{k}'} \hat{k} \hat{\Upsilon}^* \frac{\hat{\Upsilon}_-}{\hat{k}} \hat{k} \hat{\Upsilon}^* \frac{\hat{\Upsilon}_-}{\hat{p}' + \hat{k}'} \hat{\Upsilon}^* \Upsilon_- \\ &\sim \frac{\hat{k}}{(\hat{p}'' - \hat{k}')(\hat{p}' + \hat{k}')} \end{aligned}$$

FIG. 55. The tree diagram obtained from Fig. 1.

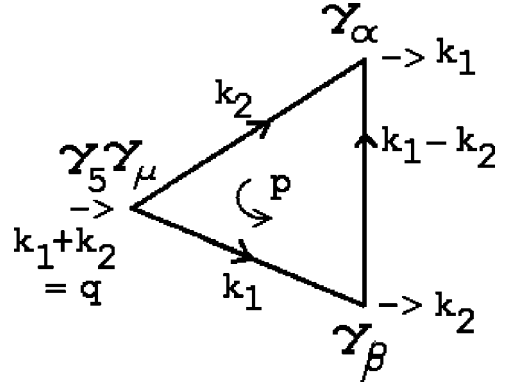


FIG. 54. The fermion loop contribution to $T_{\mu\alpha\beta}(k_1, k_2)$.

while the diagram with the arrow reversed contributes to the A_{+-} helicity amplitude. By similar reasoning, the diagram of Fig. 2 contributes to the A_{-+} helicity amplitude.

The diagram shown in Fig. 51(b) is the only possibility for the scattering of states with equal, negative, helicities. In the cross channel, in which the incoming and outgoing, right hand, vector mesons are interchanged, the diagram untwists to become the diagram of Fig. 50(a). Figure 51(b) contributes to the A_{--} helicity amplitude, while the corresponding diagram with the quark arrow reversed contributes to the A_{++} helicity amplitude. For the amplitudes with π^0 quantum numbers in the t -channel, that we discuss in this paper, it follows from CPT invariance that

$$A_{++} = A_{--} \quad \text{and} \quad A_{-+} = A_{+-}. \quad (\text{A18})$$

Note that, in all diagrams, only same sign chirality states are exchanged.

APPENDIX B: REVIEW OF LEADING AND NONLEADING LOGS

As far as we know, the diagrams we discuss in this paper have not been discussed in detail in the literature. However, if we were to make the (wrong) assumption that the left-handed coupling does not affect the extraction of high-energy logarithms, or (more simply) if we impose a transverse momentum cut-off, there are a number of well-known results that would carry over, almost directly, into our problem. Just to put the discussion of this paper in context, we give here a very brief, nontechnical, overview [11] of these results.

All the results concern the extraction of leading and non-leading logarithms. If we organize the quark-antiquark exchange diagrams into distinct series depending on the power of α_s (the QCD coupling) involved, then typical diagrams

FIG. 56. Splitting Fig. 55.

giving such logarithms are illustrated in Fig. 52. The first series contains purely electroweak diagrams that have a logarithmic expansion in α_w (the “electroweak” coupling). The second series contains $O(\alpha_s)$ corrections to the first series, the third series contains $O(\alpha_s^2)$ corrections to the first series, etc.

All diagrams of the form shown in Fig. 52 would be expected to give high-energy amplitudes of the form

$$A(S,0) \sim \sum_{S \rightarrow \infty, n, m, r} a_{nmr} \alpha_w^n \alpha_s^m [\ln S]^r. \quad (\text{B1})$$

To make our discussion straightforward we can suppose that we, initially, introduce a transverse momentum cutoff so that we can ignore ultra-violet transverse momentum divergences—including both the anomaly power divergences that we discuss in this paper, and the logarithmic divergences that we discuss below. As a result, all the coefficients a_{nmr} can be represented as (sums of) transverse momentum diagrams of the form illustrated in Fig. 53.

With the transverse momentum cutoff in place, the first two diagrams in Fig. 52 give a leading log amplitude which contains the first diagram in Fig. 53 multiplied by $\ln S$ and a next-to-leading log amplitude which contains the same transverse momentum diagram but with no factor of $\ln S$. The third diagram in Fig. 52 gives a leading log amplitude which contains the second diagram in Fig. 53 multiplied by $\ln^2 S$ and a next-to-leading log amplitude which contains the first diagram in Fig. 53 multiplied by $\ln S$ and so on. In general, the external couplings and the internal vertices in the transverse momentum diagrams acquire more and more structure (involving loop integrals) as first leading logs, then next-to-leading logs, next-to-next-to-leading logs, etc., are included in the sum (B1).

The diagram of Fig. 2, appearing in Sec. III, is the last diagram shown explicitly in the second row of Fig. 52. It is first-order in α_s , conventionally, as noted in Sec. III, we would expect that it’s leading-log contribution would contain

the last $O(\alpha_s)$ transverse momentum diagram shown explicitly in Fig. 53—with simple vertices. This diagram being obtained by placing all vertical lines on shell, as in Fig. 5 using longitudinal momentum integrations. At the next-to-leading log level the second $O(\alpha_s)$ transverse momentum diagram should be generated and the first $O(\alpha_s)$ transverse momentum diagram, which is the diagram that appears in Fig. 1, should be generated by Fig. 2 at the next-to-next-to-leading log level.

The transverse momentum diagram of Fig. 17 is the first $O(\alpha_s^2)$ diagram appearing in Fig. 53 and would be generated, at leading log, by the first $O(\alpha_s^2)$ diagram in Fig. 53. The diagram of Fig. 20 is the second $O(\alpha_s^2)$ diagram appearing explicitly in Fig. 52. The anticipated leading log result for this diagram would be $\ln^5 S$ multiplied by the second $O(\alpha_s^2)$ transverse momentum diagram appearing explicitly in Fig. 53 and the first $O(\alpha_s^2)$ diagram in Fig. 53 would be generated at the next-to-next-to-leading log level, i.e., multiplied by a factor of $\ln^3 S$.

In the leading and nonleading-log studies of pure vector gauge theories [5] there is no problem with ultraviolet divergences, either in transverse momentum, or more generally. Only the normal (ultraviolet) divergences associated with renormalization have appeared in the nonleading-log vertices. The Ward identities of the gauge theory produce cancellations that lead always to convergent transverse momentum integrals, with the accompanying logarithms just those predicted by Regge theory. (Even though, as is very well known by now, individual Feynman diagrams produce transverse momentum divergences that, at first sight, produce additional logarithms beyond those anticipated by Regge theory.) Equivalently, the complete sum of logarithms and transverse momentum diagrams can be rearranged [2] into subseries represented by Reggeon diagrams.

When fermions are involved there is, as we already noted in Sec. III, the extra subtlety of the logarithmic divergence of fermion transverse momentum integrals [11,16]. Therefore,

FIG. 57. The amplitude obtained from the second term of Fig. 56.

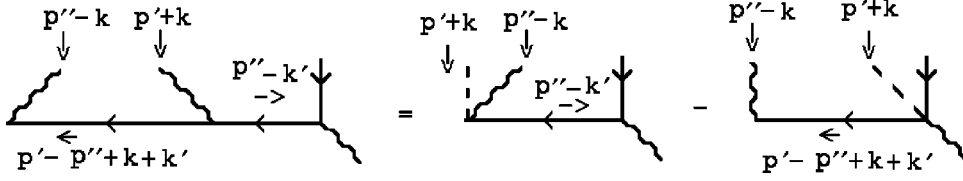


FIG. 58. Splitting of another tree diagram.

if the transverse momentum cutoff is removed, extra powers of $\ln S$ will be generated and the series (B1) must be rearranged appropriately. However, fermion Reggeization is not affected by the divergences (since the relevant transverse momentum integrals involve combinations of fermions and gluons). Consequently, as we noted in Sec. III, when the transverse momentum diagrams are organized into Reggeon diagrams, the presence of the Reggeon propagator reduces the divergence from \log to $\log[\log]$ form. Also, the Reggeon kernel for opposite sign helicities gives convergent integrals. (As we noted in the previous appendix, the distinct combinations of opposite and same sign helicities are exchanged and interact separately.) Only the kernel for opposite sign helicities (same sign chiralities) produces logarithmic divergences at large transverse momentum.

In the diagrams discussed in this paper, the quark-antiquark states we consider are same sign chirality states. However, the anomaly enhancement overwhelms the logarithmic divergence that would otherwise result. We believe this is important, physically. If we start with a transverse momentum cutoff both the anomaly power divergence and the logarithmic divergence will be absent. When the confinement and chiral symmetry breaking described in Sec. V is implemented via the extraction of infrared divergences, it may be (and the results of Ref. [8] directly suggest this) that only (transverse momentum) convergent same sign helicity exchanges are involved in forming bound states. Since “double logs” are, *a priori*, in conflict with regge theory, this is probably necessary for the bound states to be described by Regge theory.

APPENDIX C: THE ANOMALY AND VECTOR WARD IDENTITIES

To understand the special nature of Ward identities in the presence of the anomaly, it is helpful to recall some well-known properties of the one loop contribution, shown in Fig. 54, of massless fermions to an axial-vector-two-vector three current vertex $T_{\mu\alpha\beta}(k_1, k_2)$. After decomposition into invariant amplitudes

$$\begin{aligned} T_{\mu\alpha\beta}(k_1, k_2) = & A_1 \epsilon_{\sigma\alpha\beta\mu} k_1^\sigma + A_2 \epsilon_{\sigma\alpha\beta\mu} k_2^\sigma + A_3 \epsilon_{\delta\sigma\alpha\mu} k_{1\beta} \delta_1^\sigma k_2^\sigma \\ & + A_4 \epsilon_{\delta\sigma\alpha\mu} k_{2\beta} \delta_1^\sigma k_2^\sigma + A_5 \epsilon_{\delta\sigma\beta\mu} k_{1\alpha} \delta_1^\sigma k_2^\sigma \\ & + A_6 \epsilon_{\delta\sigma\beta\mu} k_{2\alpha} \delta_1^\sigma k_2^\sigma \end{aligned} \quad (C1)$$

the vector Ward identities

$$k_1^\alpha \Gamma_{\mu\alpha\beta} = 0, \quad k_2^\beta \Gamma_{\mu\alpha\beta} = 0 \quad (C2)$$

require

$$A_2 = k_1^2 A_5 + k_1 k_2 A_6, \quad (C3)$$

$$A_1 = k_2^2 A_4 + k_1 k_2 A_3. \quad (C4)$$

The large momentum region (with appropriate regularization) gives an “anomaly” contribution to A_1 and A_2 of the form

$$T_{\mu\alpha\beta}(k_1, k_2) = \frac{1}{4\pi^2} \epsilon_{\sigma\alpha\beta\mu} k_1^\sigma + \frac{1}{4\pi^2} \epsilon_{\sigma\alpha\beta\mu} k_2^\sigma + \dots \quad (C5)$$

leading to the well-known “anomalous” divergence equation

$$(k_1 + k_2)^\mu T_{\mu\alpha\beta} = \frac{1}{2\pi^2} \epsilon_{\delta\sigma\alpha\beta} k_1^\delta k_2^\sigma. \quad (C6)$$

For the vector Ward identities to hold in the presence of Eq. (C5), there must be related, infrared singular, contributions to the other A_i . For example, when $k_1^2 = 0$, Eq. (C3) becomes

$$A_2 = k_1 k_2 A_6 = \frac{q^2 - k_2^2}{2} A_6 \quad (C7)$$

implying that there must be a pole in A_6 , arising from the region of small internal momentum. In appropriate circumstances, this pole can be interpreted as a Goldstone boson pole, signaling chiral symmetry breaking.

If we consider $k_1 \rightarrow 0$, and assume that all the A_i are sufficiently nonsingular, then Eq. (C1) gives

$$T_{\mu\alpha\beta}(k_1, k_2) \xrightarrow{k_1 \rightarrow 0} A_2 \epsilon_{\sigma\alpha\beta\mu} k_2^\sigma, \quad (C8)$$

which, if we keep only the ultraviolet anomaly term (C5), gives

$$T_{\mu\alpha\beta}(k_1, k_2) \xrightarrow{k_1 \rightarrow 0} \frac{1}{4\pi^2} \epsilon_{\sigma\alpha\beta\mu} k_2^\sigma \neq 0. \quad (C9)$$

Alternatively, if we use Eq. (C3), together with Eq. (C8), we obtain

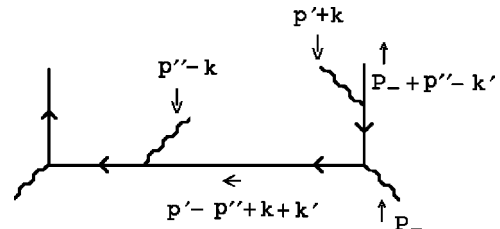


FIG. 59. Another tree diagram.

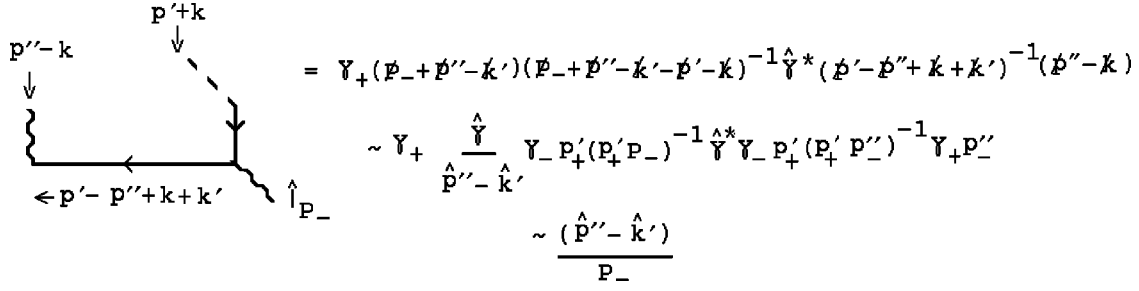


FIG. 60. Part of the tree diagram appearing in Fig. 59.

$$T_{\mu\alpha\beta}(k_1, k_2) \xrightarrow{k_1 \rightarrow 0} (k_1^2 A_5 + k_1 k_2 A_6) \epsilon_{\sigma\alpha\beta\mu} k_2^\sigma \rightarrow 0. \quad (\text{C10})$$

For consistency, again, there must be infrared singular contributions to $T_{\mu\alpha\beta}(k_1, k_2)$ that cancel the ultraviolet anomaly contribution (C5) and produce the ‘‘Ward identity zero’’ (C10).

From our point of view, therefore, the presence of the ultraviolet anomaly (C5) has two consequences. The first is the anomalous Ward identity (C6). The second is that the vector Ward identities require a cancellation between separate contributions (with different kinematic structure) from large and small internal momentum regions. As a consequence, if an explicit ultraviolet cutoff is introduced, Eq. (C5) will be modified and the vector Ward identities will no longer hold. The contribution, to the vector current divergence, of the pole term in A_6 will survive, however, since it is generated in the infrared region [8].

APPENDIX D: ELECTROWEAK WARD IDENTITY CANCELATIONS

In this appendix we consider whether Ward identity cancellations can remove the longitudinal polarization contributions of vector mesons that produce the anomaly enhanced high-energy behavior in the diagrams we have discussed. As described in Sec. III C, we are interested in Ward identity implications when we add all the diagrams that effectively replace the tree diagram that forms the lower part of Fig. 1 by another tree diagram. As in Sec. III, it will be sufficient for our purposes to consider only the diagrams of an Abelian theory.

We focus on the same region of phase space as in Sec. III, which will be the basis for all approximations we make. If we ignore $(1 - \gamma_5)$ factors (which are irrelevant for the present discussion), the lower part of Fig. 1 gives the amplitude shown in Fig. 55. We consider, first, the addition of tree diagrams in which the internal left-side vector boson line is attached at all possible points. We begin with the diagrams obtained by moving this line to the right.

The subdiagram forming the left part of Fig. 55 can be split into two pieces as illustrated in Fig. 56, where the dashed line indicates that additional momentum flows in to a vertex without changing the algebraic structure. It is the Ward identity cancellation for the second piece of Fig. 56 that involves moving the vector boson line to the right. Note, first, that if we combine this term with the right-side of the

full diagram we obtain the amplitude shown in Fig. 57 and so the relevant piece of Fig. 55 is retained.

The first tree diagram obtained by moving the left side internal vector meson to the right is the second diagram appearing in Fig. 16, which is the lower part of the Feynman diagram appearing in Fig. 17. We consider the right part of this tree diagram and divide it into two pieces as in Fig. 58. The first piece gives an amplitude that directly cancels the amplitude of Fig. 57. Therefore, it would appear that the amplitude involved in the anomaly enhancement is immediately eliminated. However, there are further cancellations that remain to be discussed.

The second piece of Fig. 58 has to be combined with the contribution of the tree diagram shown in Fig. 59. Making the usual separation (into two pieces) of the right side of the tree diagram appearing in Fig. 59 and removing the piece that cancels with the second piece of Fig. 58 leaves the piece shown in Fig. 60. This piece would be zero if the vertical antiquark were exactly, and not just approximately, on-shell.

Since the amplitude of Fig. 60 goes to zero as $P_- \rightarrow \infty$, with all internal momenta fixed, it is, superficially, a nonleading asymptotic contribution. However, it has worse large transverse momentum behavior than the original amplitude of Fig. 56. In effect, we have replaced a leading asymptotic contribution that has manageable internal momentum behavior with a superficially nonleading contribution with bad internal momentum behavior. At this point, this substitution does not actually lead to any important effects, although this will not be the case for an analogous substitution that we make later. We obtain the maximal contribution from the amplitude of Fig. 60 if we use the mass-shell condition $P_- k'_- \sim (p''_- - k'_-)^2$ and combine the resulting amplitude with the second term in Fig. 56. This gives

$$\left(\frac{k_-'^2}{k_-} \right) \frac{1}{(\hat{p}' + \hat{k}') (p''_- - k'_-)}. \quad (\text{D1})$$

This amplitude does not have the growth at large k_\perp that the amplitude of Fig. 55 has and so can be neglected.

We now consider the contribution of the first term in Fig. 56. This has to be combined with tree diagrams obtained by moving the left side internal vector meson line to the left. There is only one such diagram, which is shown in Fig. 61. Normally this contribution to the high-energy limit would be ignored because an off-shell propagator carries the large P_+

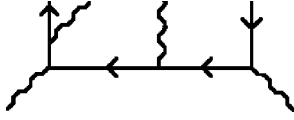


FIG. 61. Another tree diagram.

momentum. However, if we split this diagram into two pieces as in Fig. 62, the first piece cancels with the first piece of Fig. 56.

If the vertical quark line were on shell so that the full numerator, and not just the asymptotic γ_- piece, were present, the second piece of Fig. 62 would be zero. In fact, if we use the mass-shell condition $P_+ k'_- \sim (p'_\perp + k'_\perp)^2$ we obtain

$$\frac{(\hat{p}' + \hat{k}')^*}{P_+ k_-} \sim \frac{k'_- (\hat{p}' + \hat{k}')^*}{k_- (p'_\perp + k'_\perp)^2} = \frac{k'_-}{k_-} \frac{1}{(\hat{p}' + \hat{k}')} \quad (\text{D2})$$

Since both k'_- and k_- are finite in the momentum region we are considering, Eq. (D2) is of the same form as the second term in Fig. 56. In this case, therefore, a superficially non-leading asymptotic contribution, with bad large transverse momentum behavior, gives a contribution that cannot be neglected.

We now consider the additional tree diagrams that would be involved in a Ward identity for the right side internal vector meson line. From the above discussion it follows that, after we have added all such diagrams and carried out the analogous cancellations to those above, there will be one surviving contribution that will give an amplitude of the form of Fig. 55. This will come from the tree diagram shown in Fig. 63. The piece of this diagram that we have picked out would vanish if both the quark and antiquark vertical lines were on-shell. From Fig. 62 and Eq. (D2) it is clear that this piece gives a “superficially nonleading” amplitude of the form

$$\frac{(\hat{p}' + \hat{k}')^*}{P_+ k_-} \hat{k} \frac{(\hat{p}'' - \hat{k}')^*}{P_- k_+} \quad (\text{D3})$$

which, after we use the mass-shell conditions for P_+ and P_- , gives the amplitude

$$\begin{aligned} & \begin{array}{c} \text{Diagram: A horizontal line with arrows pointing left. From the left end, a vertical line goes up and then a wavy line goes right. From the right end, a vertical line goes down and then a wavy line goes left. Labels: } P_+ + k' - k \uparrow \text{ (left), } \hat{\gamma}^* \text{ (middle), } \leftarrow k' - k \text{ (right), } \uparrow P_+ \text{ (bottom left), } k + p' \text{ (top right).} \end{array} \\ & \rightarrow (\hat{k}' - \hat{k})^{-1} \hat{\gamma} (\hat{p}_+ + \hat{k}' - \hat{k})^{-1} (\hat{k} + \hat{p}') \\ & = - [(\hat{k}' - \hat{k})^{-1} \hat{\gamma}^*] \\ & \quad + [(\hat{k}' - \hat{k})^{-1} \hat{\gamma}^* (\hat{p}_+ + \hat{k}' - \hat{k})^{-1} (\hat{p}_+ + \hat{k}' + \hat{p}')] \\ & = \begin{array}{c} \text{Diagram: A horizontal line with arrows pointing left. From the left end, a vertical line goes up and then a wavy line goes right. From the right end, a vertical line goes down and then a wavy line goes left. Labels: } \hat{k} \text{ (middle), } \hat{\gamma}^* \text{ (middle), } \hat{\gamma}^* \text{ (middle).} \end{array} \\ & \sim \left[-\frac{1}{\hat{k}} + \frac{(\hat{k}' + \hat{p}')^*}{(P_+ k_-)} \right] \hat{\gamma}^* \hat{\gamma}^* \end{aligned}$$



FIG. 63. The tree diagram giving the surviving amplitude.

$$\left(\frac{k'_+ k'_-}{k_+ k_-} \right) \frac{\hat{k}}{(\hat{p}' + \hat{k}') (\hat{p}'' - \hat{k}')} \quad (\text{D4})$$

Since both $k'_+ k'_-$ and $k_+ k_-$ are finite, this is, indeed, an amplitude of the form of Fig. 55.

We conclude that the large transverse momentum behavior of the amplitude in Fig. 3, which combines with the loop amplitude in the top half of Fig. 1 to give the anomaly, does not cancel after the imposition of Ward identities. In this respect, therefore, nothing is gained by implementing the Ward identity cancellations. However, the lack of cancellation is entirely due to the asymptotic on-shell nature of the quark and antiquark lines. This raises a general issue of principle. Including the remaining amplitude that would put these lines exactly on-shell would apparently cancel the behavior (D4). Yet this amplitude would normally be neglected as contributing only to nonleading high-energy behavior. It can contribute to the leading behavior only if there are large transverse momentum divergences. In fact, as we have emphasized, to carry out the Ward identity cancellations we have actually included several diagrams that would normally be considered nonleading.

The normal procedure is to effectively assume in advance (and then justify *a posteriori*) that transverse momenta will be sufficiently cutoff after the summation over all diagrams. The leading parts of diagrams can then be safely extracted without worrying about transverse momentum divergences. The occurrence of the anomaly enhancement phenomenon in the diagrams that we have discussed could imply that in many other diagrams large transverse momenta are also sufficiently important that the normal methods are inadequate. If this is the case, then it is likely that the general transverse momentum diagram formalism will fail. Since there would then be no Reggeon diagram formalism, t -channel unitarity is also likely to fail. The conclusion, which is really the main conclusion of this paper (as we already stated in Sec. VIII), is that to use the transverse momentum diagram formalism (and therefore to ensure t -channel unitarity) it is essential to initially employ a transverse momentum cutoff.

FIG. 62. Splitting the diagram of Fig. 61.

- [1] V. S. Fadin, E. A. Kuraev, and L. N. Lipatov, *Sov. Phys. JETP* **45**, 199 (1977).
- [2] J. B. Bronzan and R. L. Sugar, *Phys. Rev. D* **17**, 585 (1978); this paper organizes into Reggeon diagrams the results from H. Cheng and C. Y. Lo, *ibid.* **13**, 1131 (1976); **15**, 2959 (1977).
- [3] V. S. Fadin and V. E. Sherman, *Sov. Phys. JETP* **45**, 861 (1978).
- [4] V. S. Fadin and L. N. Lipatov, *Nucl. Phys.* **B406**, 259 (1993).
- [5] V. S. Fadin and L. N. Lipatov, *Nucl. Phys.* **B477**, 767 (1996), and further references therein.
- [6] J. Bartels, *Z. Phys. C* **60**, 471 (1993), and references therein.
- [7] A. R. White, *Int. J. Mod. Phys. A* **8**, 4755 (1993).
- [8] A. R. White, *Phys. Rev. D* **66**, 056007 (2002).
- [9] A. R. White, *Phys. Rev. D* **66**, 045009 (2002).
- [10] A. R. White, *Phys. Rev. D* **29**, 1435 (1984).
- [11] For a detailed review and further references, see R. Kirschner, *Nucl. Phys. B (Proc. Suppl.)* **51C**, 118 (1996).
- [12] G. 't Hooft, *Nucl. Phys.* **B33**, 173 (1971).
- [13] S. I. Adler and W. B. Bardeen, *Phys. Rev.* **182**, 1517 (1969).
- [14] A. R. White, *Phys. Rev. D* **58**, 074008 (1998).
- [15] A. A. Migdal, A. M. Polyakov, and K. A. Ter-Martirosyan, *Zh. Eksp. Teor. Fiz.* **67**, 84 (1974); H. D. I. Abarbanel and J. B. Bronzan, *Phys. Rev. D* **9**, 2397 (1974).
- [16] R. Kirschner, L. Mankiewicz, A. Schafer and L. Szymanowski, *Z. Phys. C* **74**, 501 (1997).